IEET

International Electrical Engineering Transactions

Vol. 2 No. 1 (2)
January - June, 2016
ISSN 2465-4256

An online publication of the EEAAT
Electrical Engineering Academic Association (Thailand)
www.journal.eeaat.or.th

IEET – International Electrical Engineering Transactions

This journal is an online publication of the EEAAT, Electrical Engineering Academic Association (Thailand). IEET is published twice a year, ie., the first issue is for January – June and the second issue is for July – December.

EEAAT Journal Committee

Athikom Roeksabutr (Chairman)
Apirat Siritaratiwat
Kosin Chamnongthai
Prayoot Akkaraekthalin

IEET Editor

Somchai Hiranvarodom
Boonyang Plangklang

IEET (International Electrical Engineering Transactions) is published twice a year. Original contributions covering work in all aspects of electrical science, technology, engineering, and applications will be peer-reviewed by experts before publication. Topics of interest include the following: electrical power, electronics, telecommunication, control and system, sensor and measurement, optical technology, computer, information and communication technology (ICT), signal processing, social network tools and applications (apps), engineering education and other related fields.

For online submission of all manuscripts, correspondences, and letters, please visit
www.journal.eeaat.or.th

IEET Editorial Office

EEAAT - Electrical Engineering Academic Association (Thailand)
Room 409, F-Building,140 Cheum-Sampan Rd.
Nong Chok, Bangkok, Thailand 10530
Tel: +662-988-3655 ext 2216 Fax: +662-988-4026

IEET - International Electrical Engineering Transactions
Volume 2
Number 1 (2)
January – June 2016

PAPERS

Sliding-Mode Control for Four Switches Single Phase AC-AC Converter

Suwat Kitcharoenwat and **Saichol Chudjuarjeen**

Manuscript received March 29, 2016
Revised May27, 2016

ABSTRACT

This paper presents a sliding-mode control single-phase ac-ac converter with power factor control. The proposed converter can be operated in either buck or boost mode. The control algorithms operate the converter under a wide range of operating output voltage, low harmonic distortion of ac input current and improved power factor. The closed-loop system improves regulation, sensitivity to disturbances, and transient response both input current and output voltage control. The closed loop controls consist of two main parts: dual dc voltage controls of two dc-link capacitors and ac output voltage control. Simulation results verify the performance of the proposed converter and verified the proposed system that the converter is capable of input current control and regulate a wide range of output voltage.

Keywords: *Sliding-mode control, ac-ac converter, continuous current mode (CCM), power factor, single-phase ac-ac converter, buck-boost capability.*

1. INTRODUCTION

A single-phase ac-ac converter is widely used in industry, replacing auto-transformer in order to improve the ability of ac output control performance. In literatures, various topologies of single-phase ac-ac converters have been reported such as three-leg ac-ac converters, ac-ac chopper, resonant converter and ac-ac Z-source converter. The full-bridge and half-bridge structures are among the popular choices in the UPS applications (1-phase or 3-phase applications). These topologies consist of three parts namely, rectifier, dc bus controller and output voltage drivers. The three-leg acac converters have the main disadvantage of using a high number of switches. The buck type ac-ac chopper controls the ac output voltage by chopping the ac input voltage. However, this topology would produce a distortion on the ac output voltage at the zero-crossing and the operation limitation is the lack of the operation in the boost mode. The resonant converter topology converts an ac signal to another form of ac signal through the resonance of the stored energy in the inductors and capacitors. Three bidirectional switches operate at high switching frequency with low switching loss. The quantum series resonant converter is suitable for such a system with fixed voltage conversion ratio. As for the ac-ac Z-source converter, the z-source network is primarily used to store the energy. Major disadvantages are complexity of the circuit topology, ac output voltage distortion, and poor transient response.

Suwat Kitcharoenwat and **Saichol Chudjuarjeen** are with the Renewable Energy Research Unit, Faculty of Engineering, Rajamangala University of Technology Krungthep, Thailand and Dept. of Electrical Eng., Faculty of Engineering, Rajamangala University of Technology Krungthep, Thailand

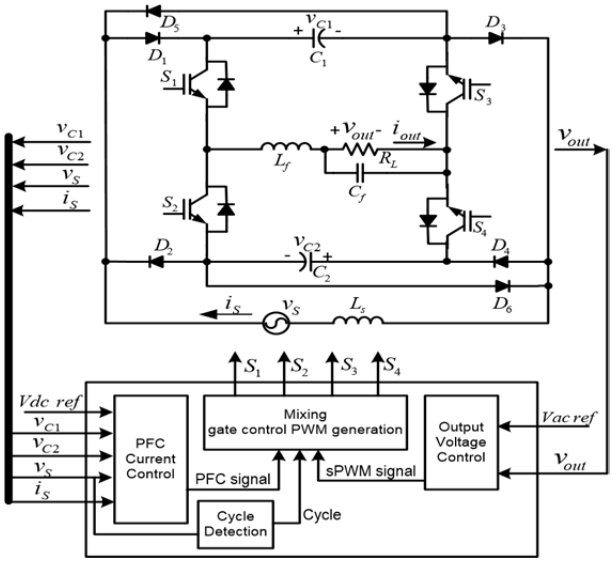

Fig.1 *Overall of proposed single-phase ac-ac converter*

Recently, a novel single phase ac-ac converter has been presented [1]. The novel ac-ac converter topology can be compared with the four-leg converters (two full bridges). They are the same operation both input current control and output voltage control with separated ground between input and output sides. A number of components is counted and compared between novel converter and four-leg converter.

Sliding-mode control has become the most widely used method for the control of single phase ac-ac converter [2]. The benefits of using this control method include robustness against system-parameter variations and external large-signal disturbances. The properties have been verified in a broad range of applications, including dc/dc voltage regulators, unity-power-factor ac/dc rectifiers, and dc/ac converters. However, the application of this control technique to novel ac-ac converter [1] has not been previously reported in

literature. This paper introduces a control-oriented model for the single phase ac-ac converter reported in [1]. Sliding-mode control theory is used to control the input current control and output voltage control for this purpose.

In this paper, the proposed sliding-mode control for single-phase ac-ac converter is designed with the following key improvements: ability to operate in buck and boost modes, ac output voltage regulation with improved transient responses, dc-link voltage control capability, ac input current waveform control with low output voltage distortion, and a minimum number of required devices. The converter circuit configuration is shown in Fig.1. The converter uses four switches to control the output voltage and the input current. The output voltage is generated by using sinusoidal pulsewidth modulation (sPWM) technique to generate pulses from the dual dc-link capacitors. The operation of the switches controls the output voltage and input current to the desired values. The gate control signals are created from two close-loop controls, the output voltage and the input current.

2 PROPOSED CONTROL

The proposed system is shown in Fig.1. The ac-ac converter topology consists of four main switches (S_1S_4), two dc-link capacitors(C_1 and C_2), an inductor (L_s), diodes (D_1 - D_6). In the system, the V_{C1}, V_{C2} , i_s and v_s are measured and fed back to the digital controller. The dc-link capacitor (C_1) is charged and $V_{C1}$is maintained constant during the positive cycle of v_s while the capacitor voltage V_{C2} is charged and maintained constant during the negative cycle. The input voltage is used as the reference signal for controlling the input current, i_s. The output current is regulated by the switches S_1 and S_3 during the positive pulse while the switches $S_2$and S_4 operate during the negative pulse, using the sinusoidal PWM (*SPWM*) technique.

2.1 INPUT CURRENT CONTROL

This section aimed to control the dc-link voltages across the capacitors C_1 and C_2 by rectifying the input voltage. The dc voltage level is boosted to the desired level while the power factor is maintained close to unity. Fig. 2 shows the equivalent circuit of the boost converter. When the input voltage is positive, the inductor L_S is charged through both switches S_1 and S_2. After the switches S_1 or S_2 are turned off depending on the output cycle, the energy storage in the inductor L_S is discharged to the dc-link capacitor C_1. Similarly in Fig. 3, during the negative half cycle of the input voltage, the inductor L_S is charged through the switches S_3 and S_4, and discharged to the dc-link capacitor C_2 by turning off switches S_3 or S_4.

The kirchhoff's voltage law in Fig.2 and Fig.3 when the charging the inductor current in positive cycle and negative cycle of ac voltage input is expressed as

$$v_s + L_s \frac{di_s}{dt} = 0 \quad (1)$$

The inductor current discharging in positive cycle is expressed as

$$v_s + L_s \frac{di_s}{dt} - \frac{1}{c_1}\int i_s dt = 0 \quad (2)$$

Likewise, in the negative cycle, the inductor current discharging can be expressed as

$$v_s + L_s \frac{di_s}{dt} - \frac{1}{c_2}\int i_s dt = 0 \quad (3)$$

2.2 AC VOLTAGE OUTPUT CONTROL

The output voltage control uses the bipolar sPWM technique by turning on switches S_1 and S_3 to apply the positive voltage from the dc-link capacitor C_1 to the output, and turning on the switches S_2 and S_4 to apply the negative voltage from dc-link capacitor C_2 to the output.

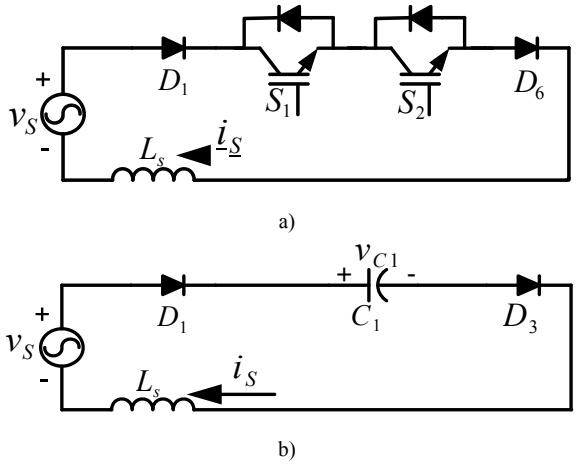

Fig. 2 *Positive cycle a) charging and b) discharging inductor current.*

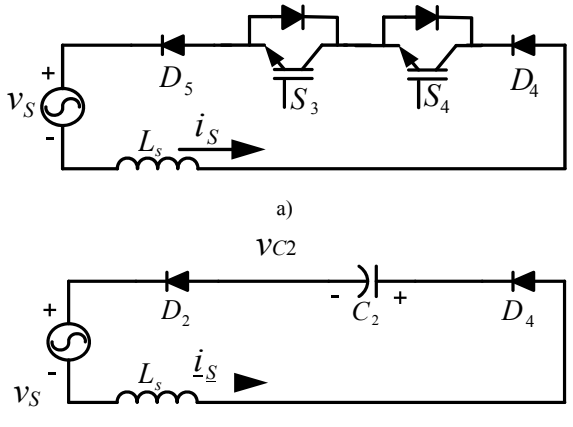

Fig. 3 *Negative cycle a) charging and b) discharging inductor current.*

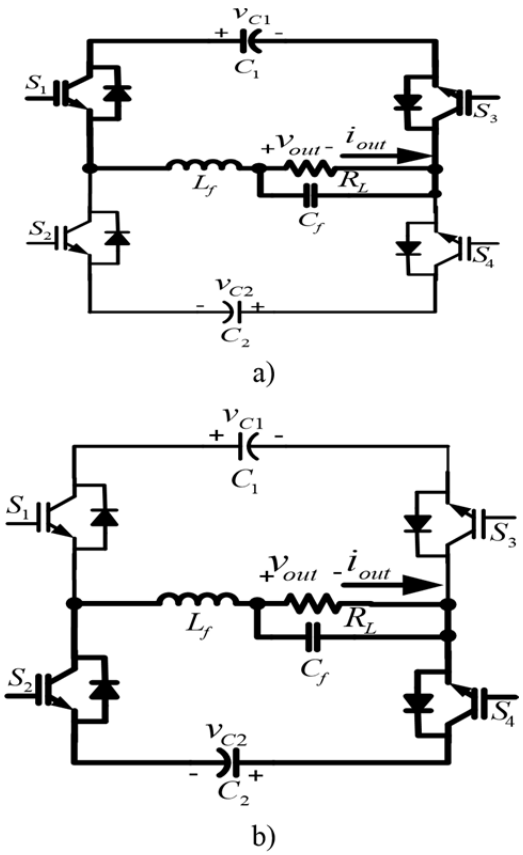

Fig. 4 *Circuit configurations under a) positive and b) negative pulses of bipolar sPWM operation.*

During positive half cycle of input voltage, the switches S_1 and S_2 are employed to control the input current. Similarly, the switches S_3 and S_4 are employed to control the input current in the negative half cycle of the input voltage. The control of output voltage is separated from the input current control. The output voltage can be set to the same or different frequencies of the input voltage.

3 PROPOSED CONTROL STRATEGY

The integrated rectifier and boost converter in the proposed system include three functions as follows.

a) Rectifying the input voltage into a dc voltage signal;

b) Boosting the dc voltage;

c) Shaping the ac input current to be sinusoidal waveform.

The control block diagram is separated into two parts. The first part is the input current control for power factor correction and the dual dc-link voltage control. The reference signal in this part is derived from the ac input voltage signal while the sliding-mode controller updates the PFC drive signal. The block diagram of this part is shown in Fig. 5.

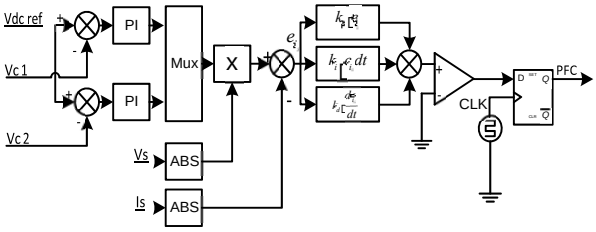

Fig. 5 *Block diagram for PFC current control*

The second block diagram is the output voltage control by using the bipolar sPWM. In this part, the sinusoidal waveform is used as the reference signal. The output voltage is sensed and fed back to compare with the reference output signal where the error is sent to the sliding-mode controller to update the sPWM signal. The block diagram of this part is shown in Fig 6.

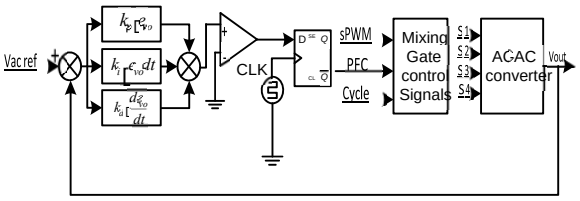

Fig. 6 *Block diagram for output voltage control*

In the mixing gate control signals block, there are two mixing controls, sPWM signals and PFC signal for ac input current control. Referring to Figure 3.12, in the mixing gate control signals block, there are two mixing controls, SPWM signals and PFC signal for ac input current control. The mixing of gate control signals can be logically expressed as follows:

$$S_1 = SPWMOR\ (PFC\ ANDCycle) \tag{3.4}$$

$$S_2 = \overline{SPWM\ OR}\ (PFCANDCycle) \tag{3.5}$$

$$S_3 = SPWM\ OR\ (PFC\ AND\ \overline{Cycle}) \tag{3.6}$$

$$S_4 = \overline{SPWMOR}\ (PFCAND\overline{Cycle}), \tag{3.7}$$

where SPWM is a digital logic signal created by the sinusoidal PWM switching scheme; PFC is a digital logic signal of the input current control; Cycle is a digital logic signal representing the positive cycle of the input voltage.

The switches S_1 and S_3 are high during positive pulse of output signals when the SPWM logic is high. On the other hand, when the SPWM logic is low (or the negated SPWM logic is high), the switches S_2 and S_4 would be high during negative pulse of the output signal. At the same time, the PFC and Cycle logics dictate the switching operation for the desired input power factor. When the Cycle signal is high, the switches S_1 and S_2

are employed to control the waveform of input current during the positive cycle of the ac input voltage. As for the negative cycle of the ac input voltage, the negated Cycle logic would be low. Then, switches S_3 and S_4 are enabled for controlling the waveform of ac input current.

4 Simulation Results

A computer simulation is performed on the proposed ac-ac converter to verify the designed performance. The following circuit parameters according in Fig.1 are shown in Table I as below. Fig. 7 shows the output voltage control under boost mode at 250Vrms/50Hz. Fig. 8 shows the simulation results of the output voltage control under buck mode at 60Vrms/50Hz. Fig. 9 shows the performance of the output voltage control with a load step from 100Ω to 60 Ω. The control performance under a step change in the output voltage is shown in Fig. 10 where the change in the reference signal is from 120Vrms to 250Vrms.

Table 1: *The simulation parameters*

Symbol	Quality	Value
Ls	inductor	10mH
C1,C2	capacitors	1,000uF
Lf	filter Inductor	1mH
Cf	filter Capacitor	10uF
Vs	ac input voltage	220V/50Hz
Vc1,Vc2	dc-link voltage	400V
Fs	Switching frequency	100kHz
Kp (PFC)	proportional gain	0.8
Ki (PFC)	integral gain	100uS
Kd (PFC)	differential gain	0.1uS
Kp (sPWM)	proportional gain	0.1
Ki (sPWM)	integral gain	500uS
Kd (sPWM)	differential gain	1uS
Vout	output voltage	0-280V

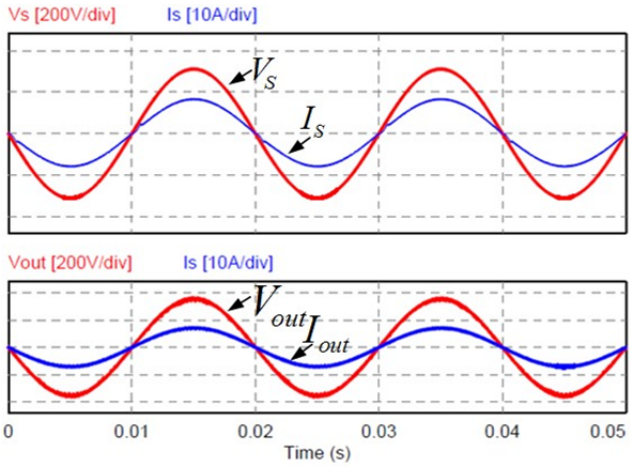

Fig. 7 *The simulation results of output voltage control in boost mode at 250V/50Hz.*

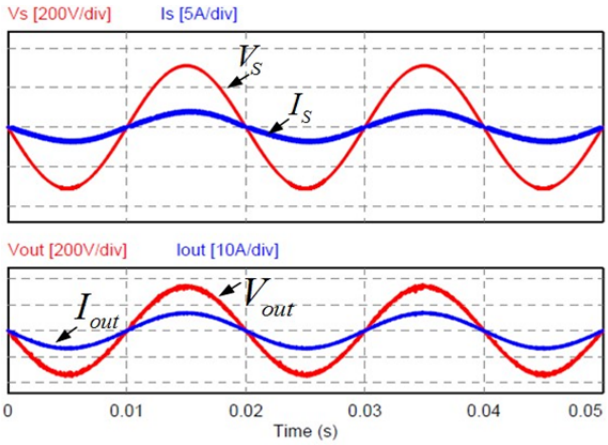

Fig. 8 *The simulation results of output voltage control in buck mode at 120V/50Hz.*

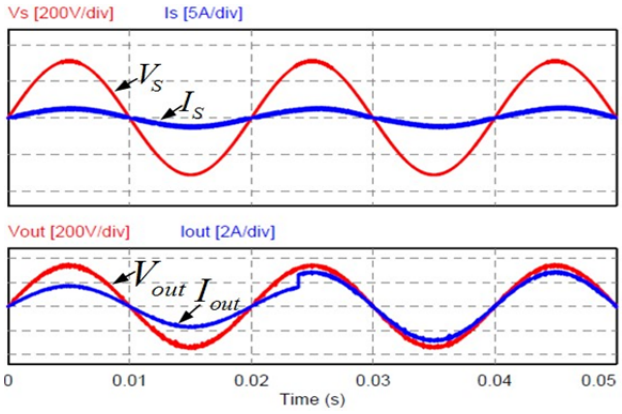

Fig. 9 *The simulation results of output voltage for step change in the load from 100Ω to 60 Ω.*

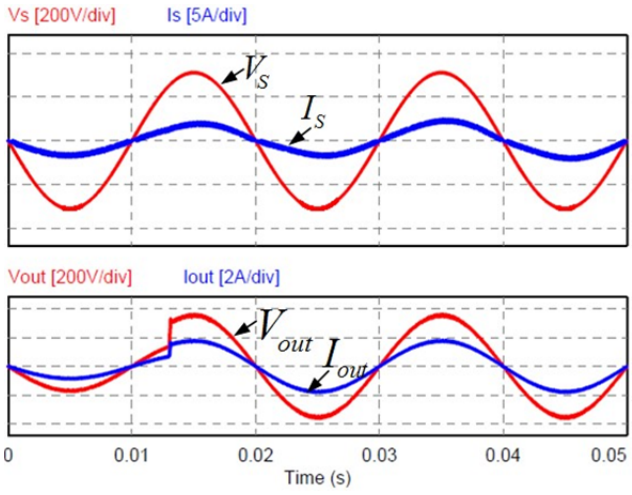

Fig. 10 *The simulation results of output voltage for step change in output voltage from 120Vrms to 250Vrms.*

4 Conclusion

The proposed topology has sinusoidal input line current with unity power factor and high quality output voltages with step change of load and step change of output voltages. The proposed topology has only four switches and operates by

the mixing gate signals from two close-loop controls. The simulation results verify fast transient response, output voltage error and load disturbances. The simulation results have been presents to verify the performance of the proposed system.

REFERENCES

[1] M.-K. Nguyen, Y.-G. Jung and Y.-C. Lim "SinglePhase AC–AC Converter Based on Quasi-Z-Source Topology," *IEEE Trans. Power Electron.*, vol. 25, no. 8, pp. 2200-2209, Aug. 2010.

[2] I. S. de Freitas, C. B. Jacobina, E. C. dos Santos, "Single-Phase to Single-Phase Full-Bridge Converter Operating With Reduced AC Power in the DC-Link Capacitor," *IEEE Trans. Power Electron.*, vol.25, no.2, pp. 272-279. Feb.2010.

[3] S. B. Bekiarov and A. Emadi, "A New On-Line Single-Phase to Three-Phase UPS Topology with Reduced Number of Switches," in *Proc. IEEE PESC*, 2003, pp.451-456.

[4] J. H. Choi, J. M. B. kwon, J. H. jung, and B. H. Kwon, "High-Performance Online UPS Using ThreeLeg-Type Converter," *IEEE Trans. Ind. Electron.*, vol. 52, no.3, pp. 889-897, Jun. 2005.

Solar Radiation Impact on Grid Power Quality for PV Grid-connected using PSCAD

Nattapan Thanomsat, Boonyang Plangklang

Manuscript received January, 2016
Revised April, 2016

ABSTRACT

This paper aims to simulate impact of radiation density on grid power quality for PV Grid-connected system. To investigate the impact, PSCAD is used to model and simulate PV array, DC converter, LC filter, AC transformer, load, and a distribution grid model. The simulation results show that if there is a change in the radiation intensity, the distribution grid system has impact factors various power quality points, such as voltage RMS, harmonic distortion, and active power. This investigation will lead to a proper design and consideration when installing the PV Grid-connected system.

Keywords: *PV Grid-connected system; Power Quality; PSCAD.*

1 INTRODUCTION

Nowadays, with the increase in use of the PV Grid-connected system, the centralized power stations have a capacity to prevent power outage points. Besides, when the PV systems are increasing this may effect power quality of the grid system [1]. In distribution systems, power quality is very important section. It is specified as the potential of the grid to supply a good and stable power to the consumers. Bad power quality will generate a problem to electrical devices and distribution unit. Several researchers studied about design a PV grid-connected system to monitor the effect of radiation to the total harmonic distortion at the point of common coupling [2]. The simulations of Solar Radiation Impact in PV system had been done in 1992, 2002, 2004 and 2005 by several researchers [3, 4, 5, 6, 7, and 8]. The present paper aims to model a PV Grid-connected system connected using Power System Computer Aided Design (PSCAD) simulation software.

2 MODELING SYSTEM

The studied PV system consists of PV array 300 kWp, DC link capacitor, inverter, LC filter connected through ac transformer with a power distribution grid. The modelled study details are shown in Fig.1 (a),(b).

The PV parameters modelled in PSCAD are shown in the Figure 2. The PV cell model used in the components is based on Dynamic Multiphysic Model for Solar Array [9]. The output power for the one module is 650 Wp and for 900 modules are 300 kWp

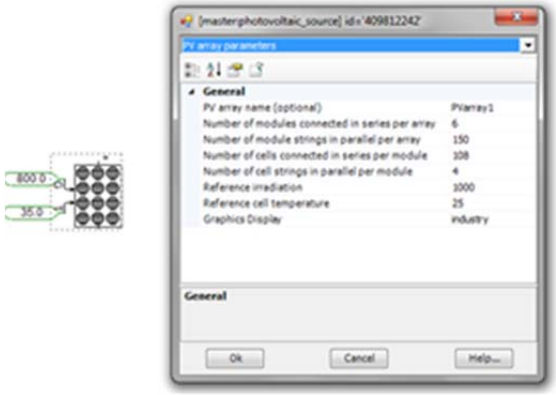

Fig.2 *Parameters of PV module in PSCAD*

DC link capacitor is an important item to reduce output power ripple. Capacitance's equation is based on a review of Power Decoupling Techniques for Micro inverters with Three Different Decoupling Capacitor Locations in PV System [10] and rounding to a typical value the DC link capacitor was sized to be 20 mF.

Several researchers studied about of Photovoltaic Array Maximum Power Point Tracking Techniques [11], comparing the instantaneous conductance (I/V) to the incremental conductance (ΔI/ΔV) can track the MPP. With the three difference cases, the MPPT creates a reference voltage (Vmpp) at that the PV array is compelled to operate. The modelled study used for creating the reference voltage Vmpp that is operated as input to DC-DC converter control model is shown in Fig. 3.

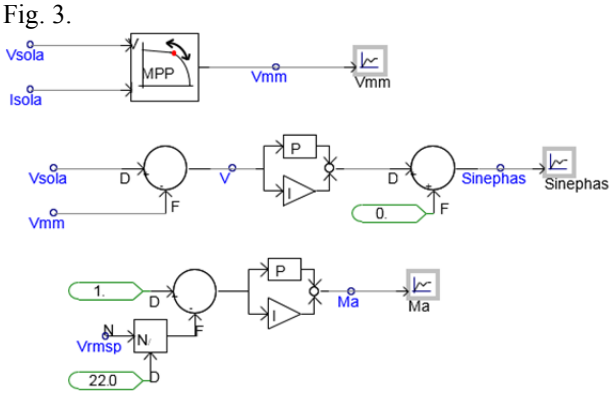

Fig. 3 *MPPT generates a reference voltage*

Nattapan Thanomsat, Boonyang Plangklang are with the Department of electrical engineering, Faculty of Engineering, 39 Moo 1, Rangsit-Nakhonnayok Road, Thanyaburi, Pathum Thani 12110 (*email: boonyang.p@en.rmutt.ac.th)

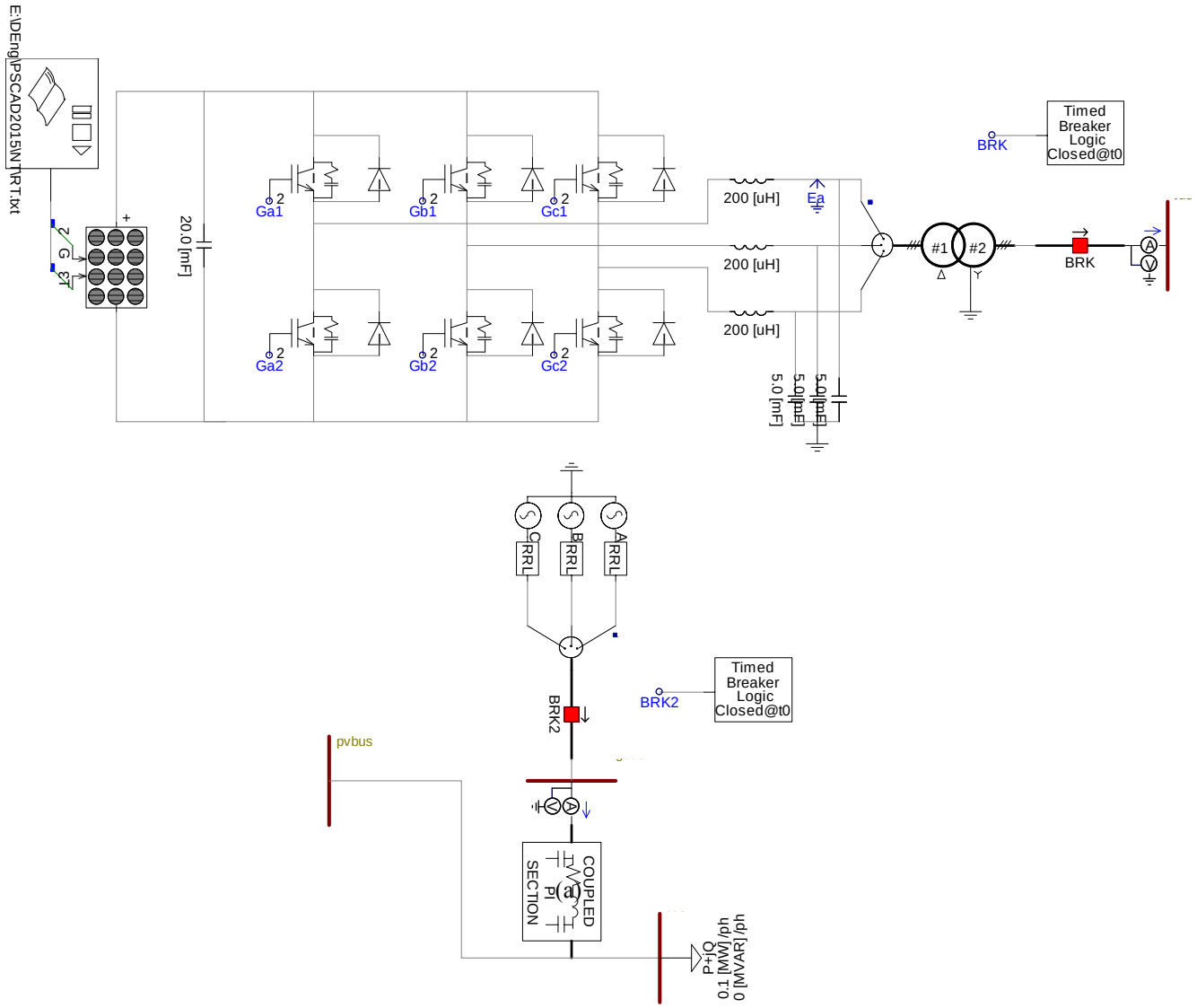

Fig. 1 *Complete grid connected PV rooftop system modelled in PSCAD (a) and (b)*

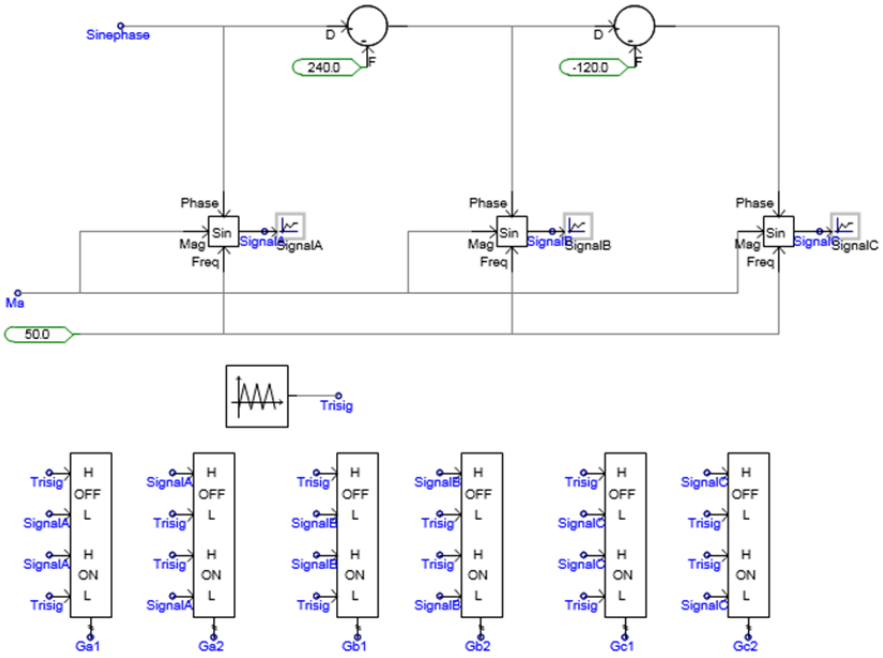

Fig.4 *DC-DC converter control model using (SPWM) technique*

The three phase inverter is composed of 6 IGBT with a snubber circuit. They transform DC power to AC with sinusoidal pulse width modulation (SPWM) technique that uses high switching frequency of 5 kHz. In Power Electronics Handbook; 2nd edition [12], the switching pulse width and switching instance can be controlled by controlling the modulating signal, which control the power flow from the inverter, and is shown in Fig. 4.

The LC filters are compelled to more smoothen the output and limit the voltage drop in the AC side of the three phase inverter when operating under varying atmosphere conditions [13].

3 RESULTS

In this simulation model, PV array that have install capacity 300 kW at STC is connected to distribution grid. The graphs are shown in Fig.5 (a), the voltage RMS, and Fig. 5 (b) the active power at the PCC.

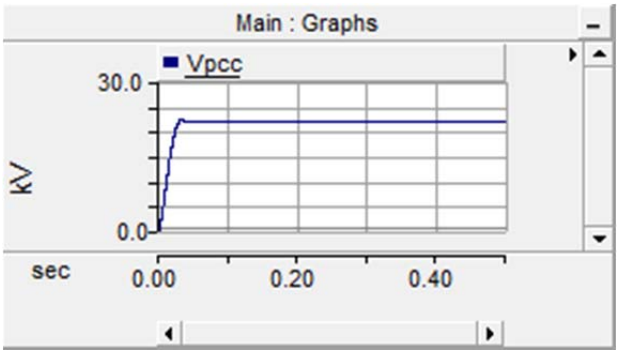

(a)

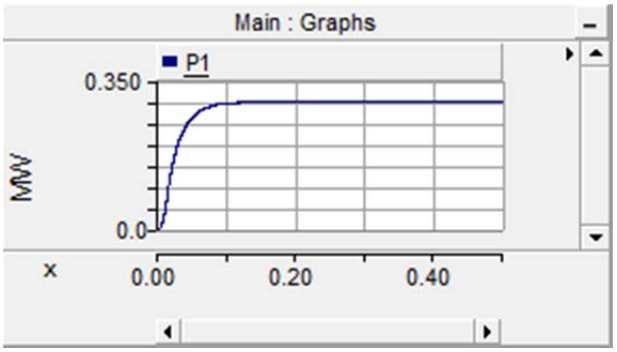

(b)

Fig. 5 *(a) the voltage RMS is maintained at PCC and (b) shows the active power at the PCC.*

In the normal day, the voltage RMS and the active power are generated with difference temperature and solar irradiation data. As illustrated in Fig.6 (a), the voltage RMS is maintained at PCC, and Fig. 6 (b) shows the active power at the PCC.

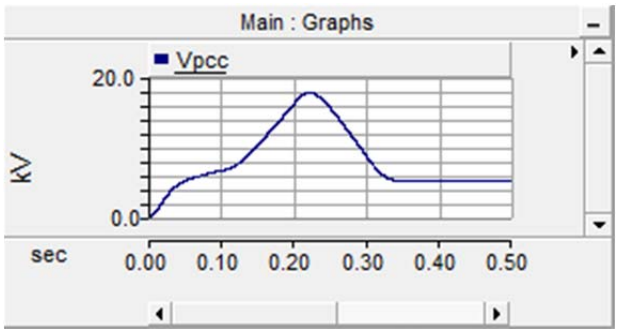

(a)

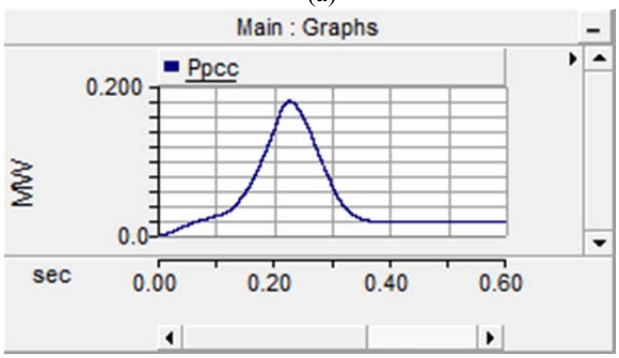

(b)

Fig. 6 *(a) the voltage RMS is maintained at PCC and (b) shows the active power at the PCC.*

In Fig. 7 (a) and (b) are shown the comparison between THDi in phase A at PCC under STC condition and with difference temperature and solar irradiation data. The graphs are display using a polymeter in PSCAD that mix the harmonic distortion (%) with its harmonic index (1-15).

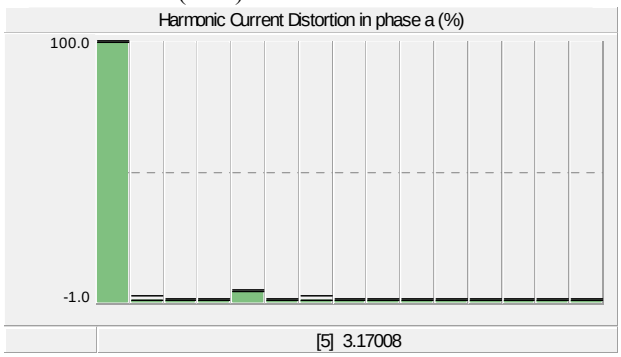

(a)

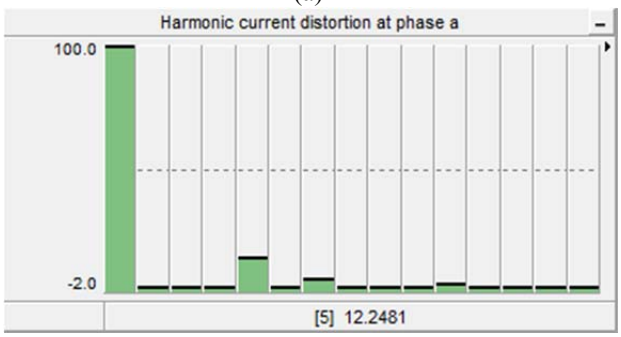

(b)

Fig.7 *(a) the THDi in phase A at PCC under STC condition and (b) under difference temperature and solar irradiation condition*

4 CONCLUSION

In this paper, the PSCAD software was selected to develop PV Grid-connected system to the power distribution grid. The impact of varying the solar irradiance and temperature condition on the PV system was simulated with developed model. The converter control module was used to generating the switching signals with SPWM for inverter. For analysis of the THDi was used by standard models in PSCAD such as FFT and Harmonic Distortion models at PCC. The simulation results show that, various power quality issues such as over voltage, under voltage, power fluctuation, and current harmonic distortion occurred in the grid power system. The study can confirm the impact of power quality on the grid system when the solar radiation is fluctuated therefore this issue must have to take in to account in order to select a proper device for the PV Grid-connected system.

REFERENCES

[1]. L. L. LOH and F. C. TZE, Distributed Generation: Induction and Permanent Magnet Generators, West Sussex, England, United Kingdom: John Wiley Y & Sons, Ltd, 2007.

[2]. A. Kalbat, "PSCAD Simulation of Grid –Tied Photovoltaic Systems and Total Harmonic Distortion Analysis", 3rd International Conference on Electric Power and Energy Conversion Systems, pp. 1-6, Oct 2013.

[3]. B. Decker, U. Jahn, U. Rindelhardt, W. Vaaben, "The German 1000-roof-photovoltaic-programme: system design and energy balance", 11th European Photovoltaic Solar Energy Conference, Montreux, Switzerland, pp. 1497–1500. 1992.

[4]. Y. Sukamongkol, S. Chungpaibulpatana, W. Ongsakul, "A simulation model for predicting the performance of a solar photovoltaic system with alternating current loads", Renewable Energy, 2002, No. 27, pp. 237-258

[5]. N. Hamrouni, M. Jraidi, A. Chérif and A. Dhouib, "Modelling, Simulation and Control of PV Pumping System", Electrimacs'2004, Hammamet, Tunisia, 2004.

[6]. A. Mellit, M. Benghanem, H. Salhi, An adaptive artificial neural network for modelling and simulation of a stand-alone photovoltaic power system, in: Proceedings of the Third Conference on Systems, Signals, and Devices, IEEE, 2005.

[7]. A. Mellit, M. Benghanem, "Modeling and simulation of stand-alone power system using artificial neural network", Solar World Congress, ISES/ASES, 2005.

[8]. Mondol, J.D., Yohanis, Y.G., Smyth, M., Norton, B., "Long-term validated simulation of a building integrated photovoltaic system", Solar Energy 78, 163–176. 2005.

[9]. Shengyi Liu and Roger A. Dougal; "Dynamic Multiphysics Model for Solar Array", IEEE Transactions on Energy Conversion, Vol. 17(2), June 2002.

[10]. H.B. Hu, S. Harb, N. Kutkut, I. Batarseh, and Z.J. Shen,"A Review of Power Decoupling Techniques for Micro inverters with Three Different Decoupling Capacitor Locations in PV System," IEEE Power Electronics, vol. 28, no. 3, pp. 2711-2726, June 2013.

[11]. T. Esram and P. L. Chapman, "Comparison of Photovoltaic Array Maximum Power Point Tracking Techniques", IEEE Trans. on Energy Conversion; vol.22; pp. 439-449, Jun. 2007.

[12]. M. H. Rashid, Power Electronics Handbook; 2nd ed.; Burlington, U.S.A.; Elsevier, 2007.

[13]. S. A. Rahman and R. K. Varma; 2011; PSCAD/EMTDC model of a 3-phase grid connected photovoltaic solar system; North American Power System; pp. 1-7.

Online Partial Discharge Detection on Power Generators

Phanupong Fuangpian, Cattareeya Suwanasri, and **Thanapong Suwanasri**

Manuscript received April 5, 2016
Revised May 31, 2016

ABSTRACT

Generator is the important part of the power system. To maintain the stability of power generator, preventive maintenance is a necessary tests and partial discharge is one of solution to diagnose insulation condition. Therefore, this paper presents the on-line partial discharge measurement and partial discharge identification on power generators. The partial discharge pattern of two 13.8 kV nominal voltage turbine generators are measured and investigated by commercial tool via capacitive coupler 80 pF. The results show that partial discharge signals and patterns can be detected in all phase of two generators. Type of partial discharge can be identified by analyzing the pattern based on phase-resolved partial discharge (PRPD). The T-F map is used to separate the phenomena for different kinds of PD source waveforms. It is found that each partial discharge phenomena in the power generators was not severe. However, the investigation on these PD must be timely observed.

Keywords: *Partial Discharge; PD Detection; Generator; TFmap*

1. INTRODUCTION

A. Partial Discharge in Generators

Partial discharge on generators mainly consists of internal discharge, surface discharge and corona discharge. Internal discharge occurs in gas gap inside the insulation. The discharge occurs when the total field inside the cavity is equal to inception field. Surface discharge occurs on insulation surfaces, due to defects between two metallic with different electric field stress. External corona discharge occurs at a sharp metallic point.. Therefore, the PD pattern on generator can be mainly classified into seven phenomena as distributed microvoids, embedded delamination, conductor side delamination, slot discharge, stress grading, sparking in air gap and bar-to-bar / bar-to-ground. Each phenomenon shows the different pattern in phase resolved partial discharge (PRPD). Generally, power producers need to be secure on electricity supply to customer. Therefore, the preventive maintenance for power generator is always needed in every 6-8 mounts. In this case, a power producer has found corona noise at generator unit 1 and suspected other PD in Generator unit 2 because of the same environment with first generator. Therefore, the investigation on partial discharge was set up to analyze the suspected problem. The results and analyzed are shown in this paper.

B. Partial Discharge Detection

Partial discharge detection can be divided into two types that are on-line measurement and off-line measurement. The on-line measurement techniques are such as High Frequency Current Transformer (HFCT), acoustic detection and Ultra High Frequency (UHF) detection while the off-line testing techniques are such as high potential (hipot) testing, IEC60270 conventional PD detector [1], power factor and dissipation factor testing, Very Low Frequency testing (VLF). Those PD detection types are used to detect the abnormal condition of the insulation system in high voltage equipments. Moreover, these tools can identify the problem's causes and severity. Then the maintenance can be properly acted.

Partial discharge detection techniques according to IEC 60270 standard [1], known as conventional method, is widely accepted with the highest accuracy. This technique can describe the phenomena of internal discharge, surface discharge, and air corona. The test circuit is represented in Figure 1. The circuit comprises coupling capacitor (Ck), noise filter (Z), input impedance of measuring system (Zmi), connecting cable, coupling device, measuring instrument and test object (Ca). Then, the discharge patterns can be observed. Some examples on discharge patterns in [2] are given in Fig. 2.

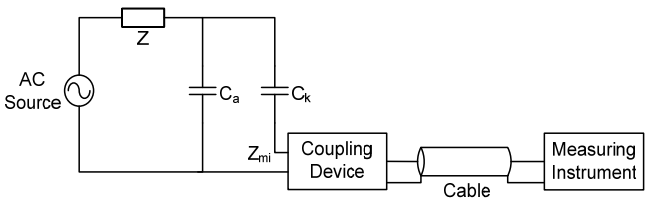

Fig. 1 *IEC* ***60270*** *standard for conventional PD test.*

Phanupong Fuangpian and Thanapong Suwanasri are with the Sirindhorn International Thai-German Graduate School of Engineering (TGGS), KMUTNB (email: phanupong003@hotmail.com)
Cattareeya Suwanasri is with Department of Electrical and Computer Engineering, Faculty of Engineering, King Mongkut's University of Technology North Bangkok (KMUTNB), Thailand

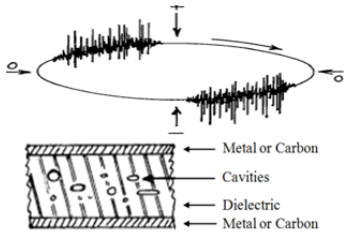

(a) Internal discharge in dielectric voids

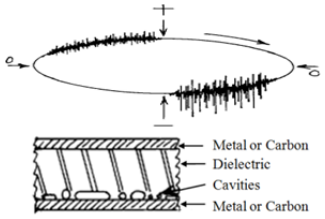

(b) Internal discharge in voids between dielectric and carbon

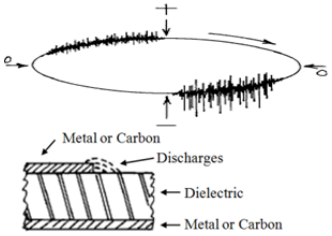

(c) Surface discharge between dielectric and carbon

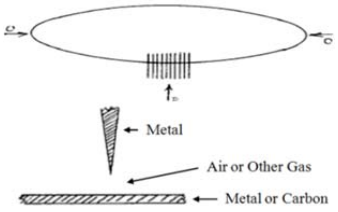

(d) Corona discharge

Fig. 2 *Partial discharge patterns*

2. ON-LINE FOR PARTIAL DISCHARGE DETECTION

In this paper, on-line partial discharge detection on power generator was observed by using unconventional diagnostic commercial tool. The testing equipment includes capacitive coupler, PD detector portable tool and connecting device.

A. Capacitive Coupler

Capacitive couplers as shown in Fig. 3 are used as the sensors to detect PD signal stator winding. They are connected with main bus bar of the generator at all three phases. The signal cables (RG58) are used to connect between capacitive coupler and Link Box outside the generator for user interface.

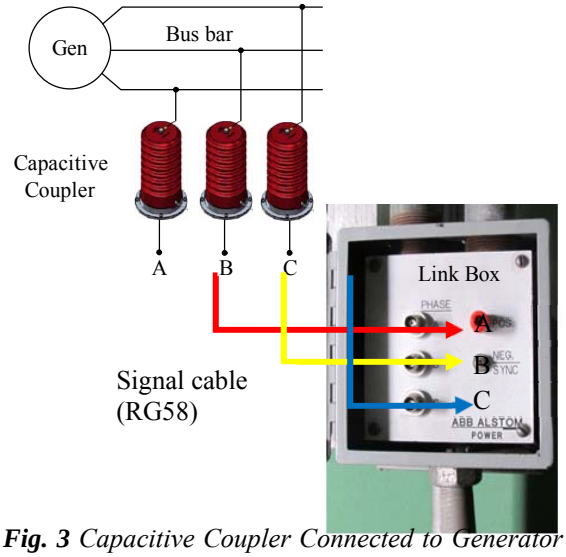

Fig. 3 *Capacitive Coupler Connected to Generator Bus bar.*

B. Measuring System for Generator Unit 1 and 2

Generators unit 1 and unit 2 are connected to Link Box via capacitive coupler with 80 pF as presented in Fig. 4 and Fig. 5. Terminal A, B, C are connected to PD detector portable tool, High Pass (HP) filter are needed for noise rejection and PD detector must be synchronized with system voltage of the generator in order to identify the partial discharge using Phase Resolved Partial Discharge (PRPD) method. The connecting cables between Link Box and PD detector portable are RG58. Moreover, the WIFI is used to connect between PD detector and computer for acquisition data. The PD software as Graphic User Interface (GUI) is used to analyze the partial discharge pattern as well as partial discharge waveform.

The specification of the PD detector portable commercial tool called the Ultra Wide Brand (UWB) digitizer is 3x100 MS/s, the bandwidth is in between 16 kHz to 35 MHz. Waveform Fast Fourier Transform (FFT) spectrum shows in real time PRPD pattern. The T-F mapping as technology is used to separate the PD phenomena. The process entire waveform of PD pulse is recorded by this tool.

C. T-F Mapping

Fast Fourier Transform (FFT) is applied to separate the signals into different frequencies and time-lengths. Later on, those signals can be plotted into T-F map [3] in order to classify types of signal such as noises or PD pulses. For example, two pluses as slow and fast pluses shown in Fig. 6, they are analyzed and plotted in T-F map as shown in Fig. 7. Finally, these phenomena located in different parts on T-F map are indentified the types of signals.

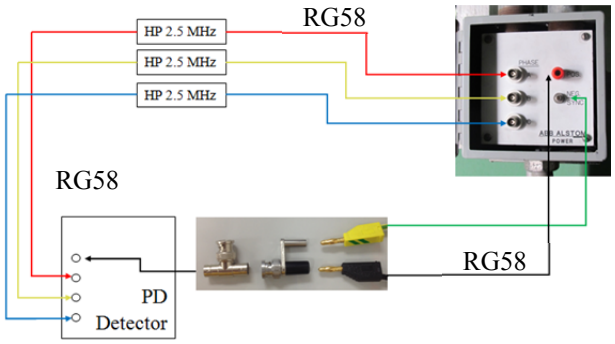

Fig. 4 *Measuring system for generator unit 1.*

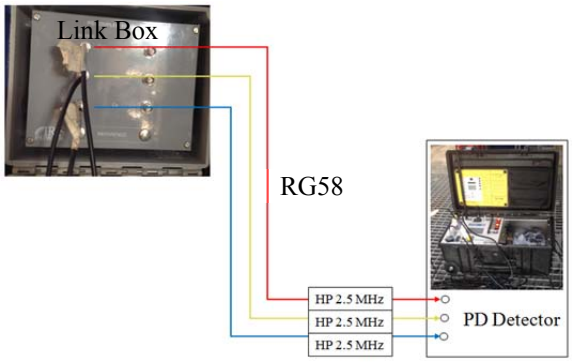

Fig. 5 *Measuring system for generator unit 2.*

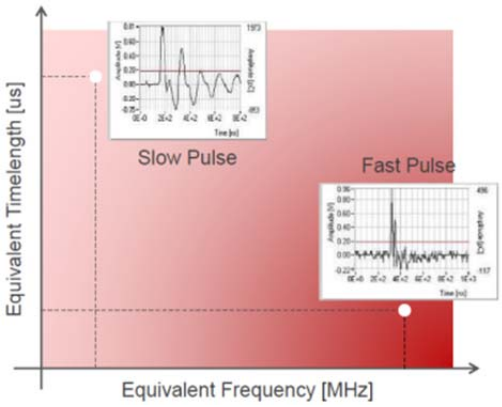

Fig. 6 *Waveforms separated by FFT.*

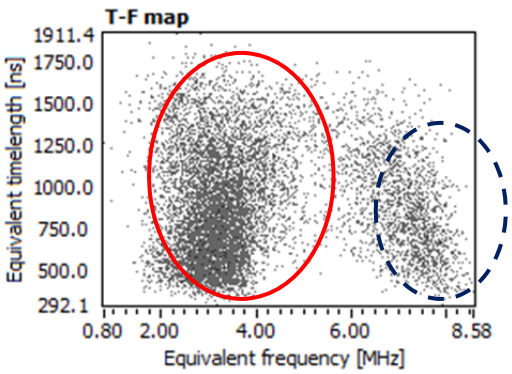

Fig. 7 *Signal phenomena in different parts on T-F map.*

3. TEST RESULTS

In this paper, two generators with rated voltage 13.8 kV were measured and investigated by using PD detector. The capacitive couplers with 80 pF were installed at the bus bar in both generators. Partial discharges signal in three phases of 2 generators were observed and investigated by using PRPD and pulse wave form. The identification was based on pattern in PRPD as worldwide technique [4].

D. Background Noise

Before any analysis, the background noise must be mitigated. They are caused by the variation in voltage from external source as well as communication signals, resulting to also cause some currents to flow between the source and the capacitance of the system being tested, even without a PD event in the test object. The background noise is detected in commercial tool. In this test, background noise lower than 5 mV was removed as shown in Fig. 8.

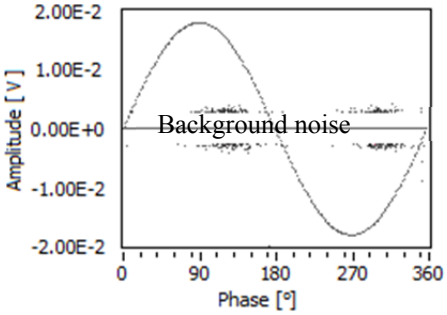

Fig. 8 *Background noise in the system.*

E. PD Detection on Generator Unit 1

For generator unit 1, the partial discharge appeared in all phase with different phenomena. In phase A, the entire PD pattern in PRPD is shown in Fig. 9 (a). This pattern can be separated into two phenomena as given in Fig. 9 (b) and (c). The cause of two phenomena is analyzed and identify to be distributed microvoids.

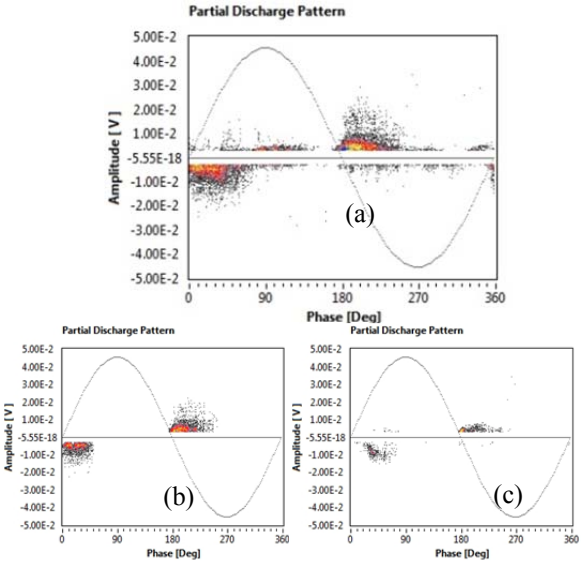

Fig. 9 *Detected signal on phase A of in generator unit 1 (a) Entire pattern of detected PD (b) Phenomenon shows 1st internal PD (c) Phenomenon shows 2nd internal PD.*

In phase B, the entire PD pattern in PRPD of Phase B is shown in Fig. 10 (a). Similarly, this pattern can be separated into two phenomena as given in Fig. 10 (b) and (c). The first phenomenon shows stress grading at overhang of phase B while the second phenomenon is cross-talk from phase C.

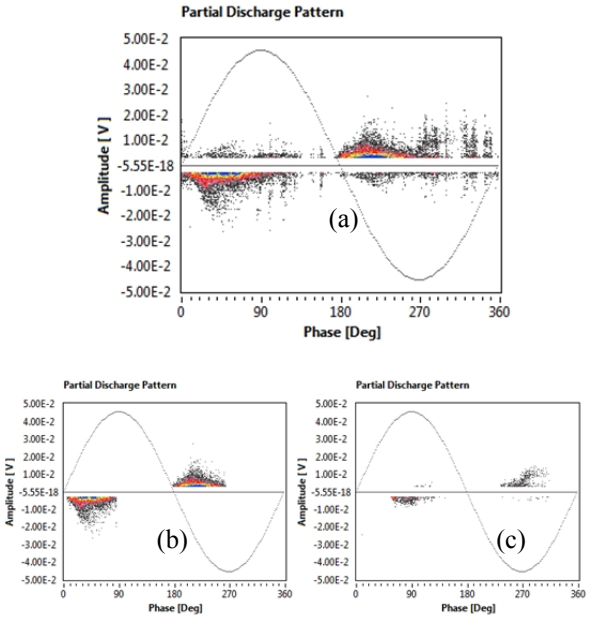

Fig. 10 *Detected signal on PHASE B of in Generator Unit 1 (a) Entire pattern of detected PD (b) 1st Phenomenon shows stress grading (c) 2nd Phenomenon is cross-talk from another phase.*

In phase C, the entire PD pattern in PRPD of Phase B is shown in Fig. 11 (a). Similarly, the pattern can be separated into three phenomena as given in Fig. 11 (b), (c) and (d). The first phenomenon shows stress grading at overhang of phase C while the second and third phenomena are the cross-talk from phase B.

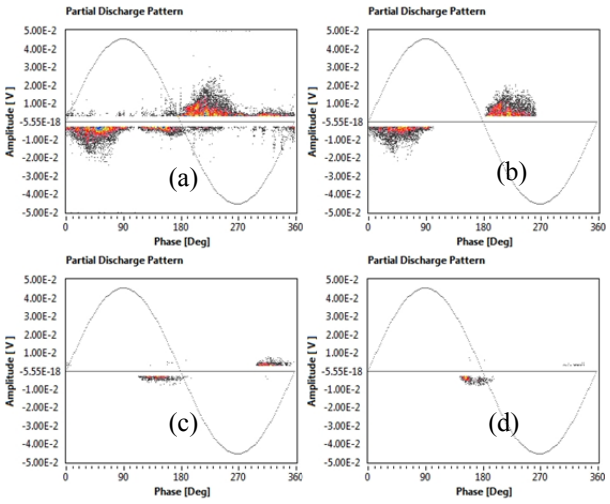

Fig. 11 *Detected signal on phase C of in generator unit 1 (a) Entire pattern of detected PD, (b) 1st Phenomenon shows stress grading, (c) 2nd Phenomenon is cross-talk from other phase, (d) 3rd Phenomenon is cross-talk from other phase.*

F. PD detection on Generator 2

For generator unit 2, the partial discharge appeared in only phase A and C. All patterns are shown in PRPD. In phase A, two phenomena of distributed microvoids were detected as shown in Fig. 12 (b) and (c). For phase B, only cross-talks form phase A were appeared as shown in Fig. 13 (a) - (d). In phase C, the partial discharge is a discharge in air gap between busbars and pressure finger in the region as shown in Fig. 14.

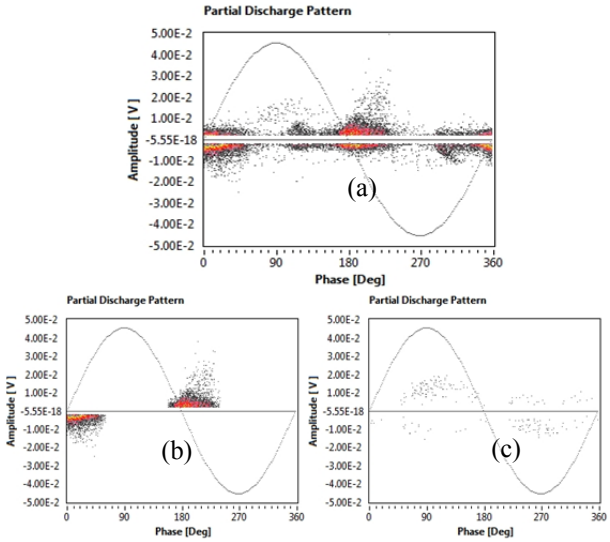

Fig.12 *Detected signal on phase A of in generator unit 2 (a) Entire pattern of detected PD (b) Phenomenon shows 1st internal PD (c) Phenomenon shows 2nd internal PD.*

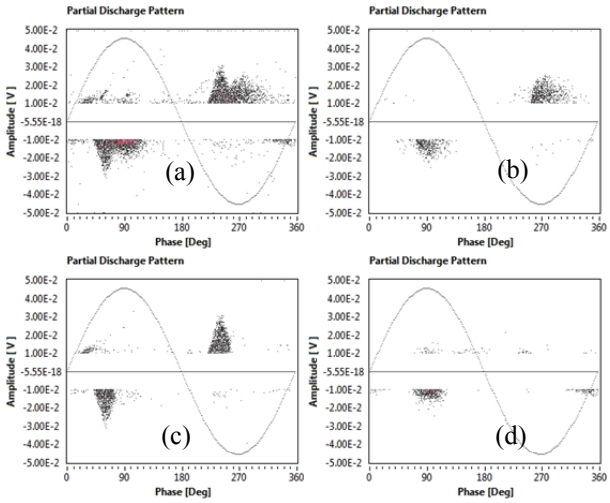

Fig.13 *Detected signal on phase B of in generator unit 2 (a) Entire pattern of detected PD, (b) 1st Phenomenon is cross-talk from other phase, (c) 2nd Phenomenon is cross-talk from other phase, (d) 3rd Phenomenon is cross-talk from other phase.*

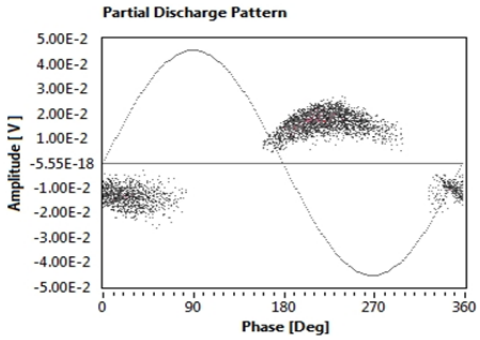

Fig.14 *Detected signal on phase C of in generator unit 2*

G. Problem Resolving

In this case, the amplitude of PD signals is not high. Therefore, the trend of PD needs to be observed closely. Then, if the partial discharge has higher amplitude and repetition rate the visual inspection is needed to take action.

Nowadays, the PD monitoring is used to be a system for observing the insulation system of the power generator and for alarming to a Central Unit (CU) placed in the utility headquarter [5].

4. CONCLUSION

The capacitive couplers are used to be sensors for partial discharge detection on power generators. Two power generators as nominal voltage 13.8 kV were investigated. The partial discharges from different sources and noises on entire PD pattern were separated by using T-F map. In field measurement, the background noise is not stable like in laboratory. Then, the noise should be rejected to clearly show the PD pattern to identify the correct results. The distributed and stress grading were found in both generators with low amplitude. In the conclusion, the defect caused from insulation aging can cause the degradation of power generator because of high electric stress, mechanical stress and partial discharge initiation. Therefore, the life extension of generator can be achieved by the good maintenance as condition based-management.

5. ACKNOWLEDGMENT

The authors thank the An independent power producer for generators as well as TGM, Thailand for PD measuring tools from Techimp.

REFERENCES

[1]. IEC 60270, “High Voltage Test Techniques-Partial Discharge Measurements Edition 3”, 2000.

[2]. CIGRE Working Group 21.03, “Recognition of Discharges,” Electra, No. 11, pp. 61-98, December 1969.

[3]. A. Contin, A. Cavallini, G.C. Montanari, G. Pasini, F. Puletti, “Digital detection and fuzzy classification of partial discharge signals”, IEEE Trans. Dielectr. Electr. Insul., Vol. 9, No. 3, pp. 335-348, 2002.

[4]. Claude Hudon, Mario B´elec, “Partial Discharge Signal Interpretation for Generator Diagnostics”, IEEE Transactions on Dielectrics and Electrical Insulation, Vol. 12, No. 2; April 2005.

[5]. L. Fornasari, G.C. Montanari, A. Cavallini, “Alarm Management in permanent PD Monitoring for Generators”, Electrical Insulation (ISEI), Conference Record of the 2012 IEEE International Symposium, 2012.

Electric Vehicle Loads for Power Flow Analysis

Yuttana Kongjeen and Krischonme Bhumkittipich

Manuscript received April 20, 2016
Revised June 2, 2016

ABSTRACT

This paper proposes electric vehicle loads for power flow analysis based on User Define Models (UDMs) in power system analysis toolbox (PSAT) programming. According to the development of EV technology, the EV has totally designed and made for using in city area as city cars. To study the proposed performance, the EV load is modeled as the function box equivalent on PSAT connected to the single line diagram of power system model. The IEEE 14 bus system is selected for testing EV load model compared between PQ load base case and EV load. This proposed EV load model can be used to simulate for solving the power flow analysis under continuation power flow (CPF) method. The EV load model is directly affected to voltage stability margin when the EV load increased. Therefore, this study can be verified that proposed EV load can use to study the EV load in the future works.

Keywords: *Electric Vehicle Load; Power Flow Analysis; , Load Voltage Diaviation, Continuation Power Flow Method*

1. INTRODUCTION

Recently, the study of electric vehicle (EV) in power system has been an interested to research on electrical power system. The high penetration of EV load in the electrical power system will be important to analyze and solve power flow for tracking power system problem. The energy management system (EMS) are required to system management and optimize of energy consumption from energy sources. Because of number of EV load charger may be charged at the same time at same power grid line. Therefore, it is necessary to develop an effective EV load and to investigate the impacts on power system operation.

Fig.1 The smart grid concept is the integration of electrical and communication infrastructures with advance process automation and information technologies within the existing electrical network. Smart grid represents a complete change in the way utilities, politicians, customers, and other industry participants think about electricity delivery and its related services. Consequently, the role of EV load is coming to consume energy in demand side of grid and control from EMS. The impact of EV charging station was effected to reduce the steady state voltage stability by the modeling based on harger of EV battery. It is observed that the power voltage relationship confirms the analytically derived load characteristics consist of constant power component and voltage dependent power component [1].The EV load was evaluated of their impact on system oscillatory stability based on voltage profiles. The dependent load characteristic was found that EV load was the high impact to power system when compared to conventional PQ loads in single machine infinite bus (SMIB) [2]. The EV load from constant power without considering the voltage profile of EV charging system. The EV charging system cannot provide the accurate information about behavior of charging system during charging process. Therefore EV load is developed based on ZIP load that can be used to analyze the behavior of EV charger and integrated to a power grid and determined the impacts of EV charging load [3].A model of new plug-in electric vehicles (PEVs) for power flow studies based on voltage source converter (VSC) and PEV active power from instantaneous state of charge and discharge is proposed in [4]. The PEVs were effected to voltage profile and can improved voltage stability on power system. The experimental results on laboratory scale measured and derived the model of new load subject to the large voltage change and theirs effect on voltage stability studies based on static load model [5].The queuing theory based in a PQ bus with stochastic characteristics of electric vehicles demand system were closed formulas for real and reactive power of the EV demand system from charging time that can be found in [6].

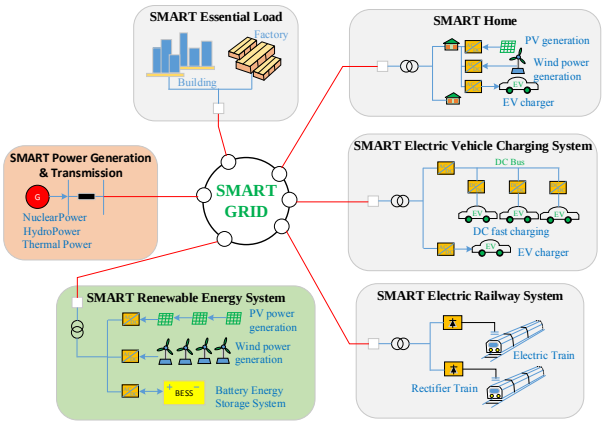

Fig.1 *The SMART grid interfaced with Electric Vehicle load*

Yuttana Kongjeen and Krischonme Bhumkittipich are with the Power System Research unit, Department of Electrical Eng. Rajamagala University of Technology Thanyaburi, phathum Thani, Thailand (Email: yuttana_k@mail.rmutt.ac.th and krischonme.b@en.rmutt.ac.th)

The rest of this paper is organized as follows: Section 2 proposes the EV load modeling for power flow analysis that consists of EV load modeling, Newton Raphson power flow with EV load, continuation power flow and load voltage deviation. User defile modeling and interface is presents in Section 3. Section 4 shows the simulation results based on IEEE 14 bus test system. Finally, the conclusion and discussion are given in Section 5.

2. EV LOAD MODELING

Fig. 2 shows the voltage dependent load characteristics that was represented of EV load model based on the group of Plug-in Electric Vehicles (PEVs) charger in power grid connection. The dc-dc convertor stage is to achieve the required charge current suitable for different state of charge condition and cell temperatures control of battery. Generally the EV load model can be shown in [1],[2] from equation (1) and in practical can be done using in equation (2) and (3), respectively. The EV load model are required parameters for completely load that came from experimental results by testing the EV fast charger.

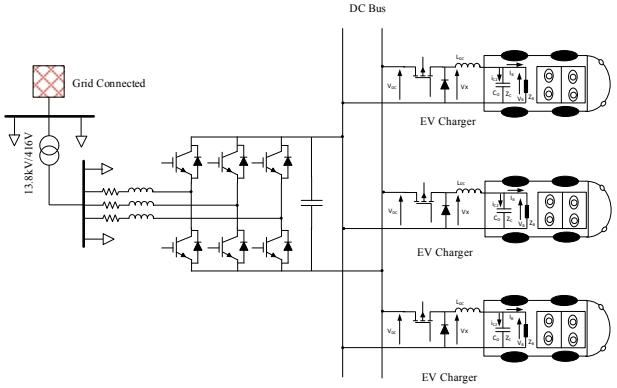

Fig.2 *The ac-dc converter at the grid interface and dc-dc converter of a PEVs charger [9].*

$$\frac{P}{P_0} = b + a\left(\frac{V}{V_0}\right)^{\alpha} \quad (1)$$

Therefore;

$$P = b + a\left(\frac{V}{V_0}\right)^{\alpha} \quad (2)$$

$$Q = P \times \tan(\theta), \quad (3)$$

where V and V_0 are the rated voltage and nominal voltage. The θ indicates the power factor of the connected load, while a, b, α are the constant power, voltage dependent power and exponential component of load, respectively. The P_0 refers to the real power consumption of load at voltage V_0. So that the real and reactive power of EV load are given by P and Q, respectively.

3. NEWTON RAPHSON POWER FLOW WITH EV LOAD

The EV load identified voltage dependent load (VDL) characteristics. Therefore, accommodating it in Newton-Raphson power flow algorithm requires certain modifications to the algorithm. The required modifications to the real and reactive power flow equations of the algorithm are shows in equation (4) and (5) [10].

$$P_{Gi} - P_{Di}(v) = v_i \sum_{k=1}^{N_B - 1} v_j \left[G_{ij} \cos\delta_{ij} + B_{ij} \sin\delta_{ij} \right] \quad 4)$$

$$Q_{Gi} - Q_{Di}(v) = v_i \sum_{k=1}^{N_{PQ}} v_j \left[G_{ij} \sin\delta_{ij} + B_{ij} \cos\delta_{ij} \right], \quad (5)$$

where δ_{ij} is the bus voltage angle between buses i and j. The total number of buses and number of load buses are represented as N_B and N_{PQ}, respectively. The injection real and reactive power at bus i are represented by, P_{Gi} and Q_{Gi}, respectively. The real and reactive power consumption of the load at bus i are given by P_{Di} and Q_{Di}, respectively. The conductance and susceptance of feeder ij are described by G_{ij} and B_{ij}, respectively. Consequently, the diagonal elements of J_2 and J_4 of standard power flow Jacobian should also be modified. The modification required are show from equation (4) and (5) in term differential equation into sparse matrix of Newton-Raphson power flow algorithm.

4. CONTINUATION POWER FLOW METHOD (CPF)

In order to study the impacts of different loading margin for sizing of PEVs in an electrical power system. Therefore, the CPF method were used to solve the standard power system model from a set of nonlinear differential algebraic equation, as follows:[11]

$$\dot{x} = f(x, y, p) \quad (6)$$

$$0 = g(x, y, p) \quad (7)$$

where $\dot{x}$ are the state variables $x \in \rightarrow \mathbb{R}^n$, y are the algebraic variables $y \in \rightarrow \mathbb{R}^m$, p are the independent variables $p \in \rightarrow \mathbb{R}^l$; f are the differential equations $f: \mathbb{R}^n \times \mathbb{R}^m \times \mathbb{R}^l \mapsto \mathbb{R}^n$, and g are the algebraic equations $g: \mathbb{R}^m \times \mathbb{R}^m \times \mathbb{R}^l \mapsto \mathbb{R}^m$.

The CPF method consists in a predictor step and corrector step. The inserting load parameter λ reformulate the load flow equation. The solving problems were applied parameterization technique and can be adapted real and reactive power from equation (4),(5),(6) and (7),respectively [11],[12].

$$0 = f(x, y, \lambda) \quad (8)$$

$$0 = g(x, y, \lambda), \quad (9)$$

where $\lambda \in \mathbb{R}$ is the loading parameter, which is used to vary base case generator and load powers, P_{G0}, P_{L0} and Q_{L0}, respectively, as follows:

$$P_G = (\lambda + \gamma k_G) P_{G0} \tag{10}$$

$$[P_L, Q_L] = \lambda [P_{L0}, Q_{Lo}] \tag{11}$$

5. Load Voltage Diaviation (LVD)

The LVD was used to solve the bus voltage deviation that effected from load increase into the electrical power system. The LVD need minimize value of load voltage bus can be described in equation (12) [12].

$$LVD = \sum_{k}^{n} \left(\frac{V_k^{ref} - V_k}{V_k^{ref}} \right)^2, \tag{12}$$

where V_{ref} and V_k are voltage reference in normally setting at 1 p.u. and load voltage bus, respectively.

6. User Define Models and Interface

The EV load modeling was develop from equation (2) and (3). By using User Define Models (UDMs) and interface EV model block, the simulink library was designed in PSAT program. The two parts are required relate by convert all electrical power system model and EV model test system in GUI block to M-file data for preparing the first data. The basis method are describes as below. The PSAT is selected for power system analysis which is open source program running on MATLAB and GNU/Octave based software package. The PSAT can be used to analyze and design the electrical power system for solving the complex problem [11]. The UDMs were allowed extending the capability of function model defining by user and help end-user to quick set up their own models. The UDMs of EV load model can be created by means of the GUI and EV load model on GUI of Simulink library depicted in Fig. 3.

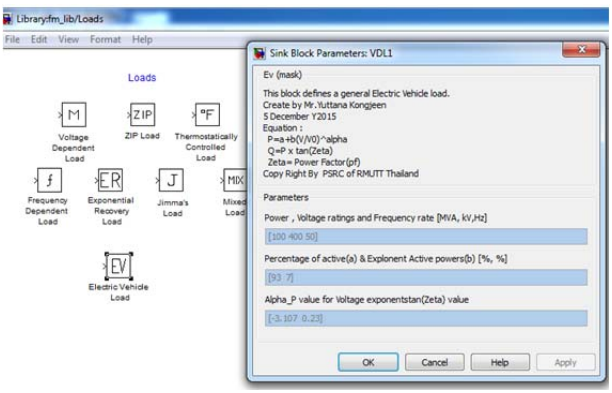

Fig.3 *The EV load model on GUI of Simulink in PSAT.*

The EV load modeling is created from UDMs function and EV load model on GUI of Simulink library in PSAT must be rerated and linked the parameters. The language programing skill for development EV load model in process of function in PSAT are required.

7. Simulation Results

The IEEE 14 bus system base case used an EV load is connected via 100MVA 13.8kV/416V step-down transformer at bus No.15 as shown in Fig.4. The EV load are represented the group of DC fast charging unit for Plug-in Electric Vehicle in distribution system. To determine the EV load from equation (1) and (2) parameter of a , b , α and power factor are 0.07, 0.96, -3.107 and $pf = 0.96$, respectively. The simulation results showed comparison of voltage profile and PV curve between base case and proposed EV load installation at bus No.15 by vary power rated of EV load 5MVA, 10MVA, 20MVA, 30MVA, 40MVA, 50MVA, 70MVA and 79MVA, respectively.

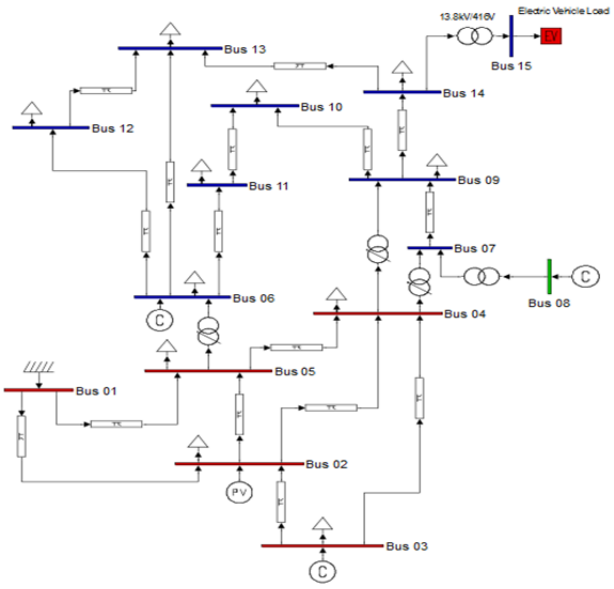

Fig. 4 *The IEEE 14 bus test system and an EV load fleet via transformer step-down at bus 15.*

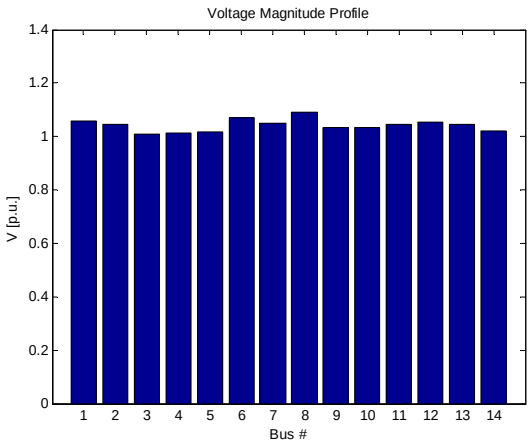

Fig. 5 *The IEEE 14 bus test system base case.*

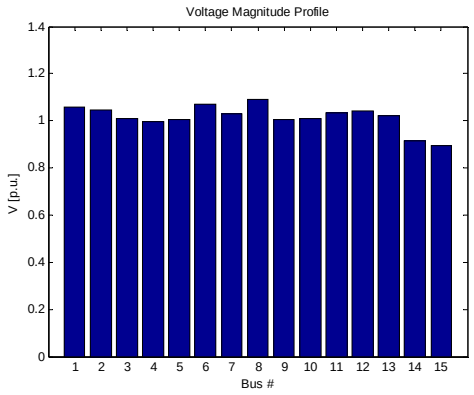

Fig.6 *The IEEE 14 bus test system and a EV load 50MVA fleet via transformer step down at bus No.15.*

The general load profile base case for the whole load is the depicted in Fig.5. It shows a load voltage of PQ load was installed in the power system. The total power loses and LVD are 0.1358 p.u., 0.2749 p.u. and 0.0313 p.u, respectively. Fig.6 showed the load voltage profile with sizing 50MVA of EV load into the power system at bus No.15 that the load voltage profile each bus are changed the total power loses and LVD are 0.2606 p.u., 0.8201 p.u. and 0.0411 p.u, respectively.

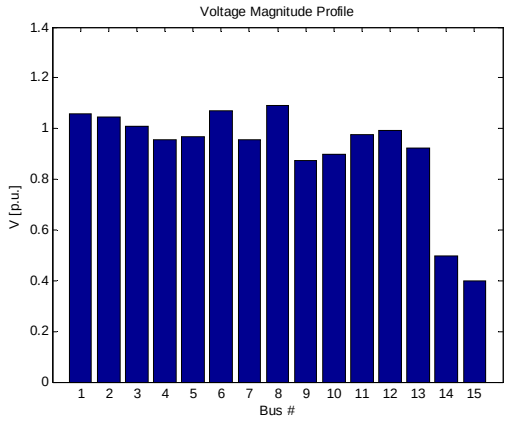

Fig.7 *The IEEE 14 bus test system and a EV load 79MVA fleet via transformer step down at bus No.15.*

Fig.7 shows the high impact of EV load that was effected to load voltage profile with sizing 79 MVA of EV load into the power system at bus No.15. The effecting voltage magnitude was directed at EV load connect to bus No.15 and other bus. The total power loses and LVD are 0.9625 p.u., 3.4328 p.u. and 0.6724 p.u, respectively.

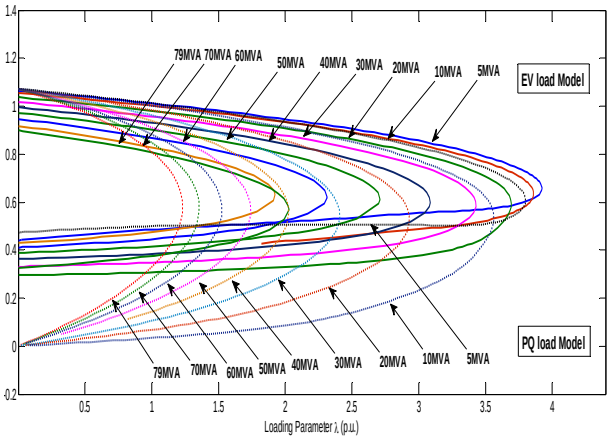

Fig.8 *PV curves by vary EV load fleet via transformer step down at bus 15.*

The simulations above to find out the PV curve by vary sizing of PQ load and EV load at bus No.15.The simulation results were compared characteristic of curve when loading any sizing. The loading margin of PV curve from EV load were changed from 4 p.u. to 1.8 p.u. opposite from direction of sizing EV load, while the loading margin of PV curve from PQ load were changed from 3.6 p.u. to 1.2 p.u.. Therefore, it is necessary to analyze loading margin and capability of power system when carrying any sizing EV load in to power system.

TABLE I. TEST RESULTS

Test Case	*Ploss (p.u.)*		*Qloss (p.u.)*		*LVD*	
	EV	*PQ*	*EV*	*PQ*	*EV*	*PQ*
IEEE 14 Bus (Base Case)	0.1358		0.2749		0.0314	
+1 EV/PQ (5MVA)	0.1435	0.1429	0.3092	0.3068	0.0304	0.0305
+1 EV/PQ (10MVA)	0.1519	0.1507	0.3469	0.3414	0.0294	0.0295
+1 EV/PQ (20MVA)	0.1715	0.1684	0.4335	0.4197	**0.0284**	**0.0285**
+1 EV/PQ (30MVA)	0.1953	0.1893	0.5378	0.5115	0.0294	0.0289
+1 EV/PQ (40MVA)	0.2244	0.2139	0.6641	0.6188	0.0331	0.0315
+1 EV/PQ (50MVA)	0.2606	0.2430	0.8202	0.7447	0.0411	0.0368
+1 EV/PQ (70MVA)	0.3760	0.3202	1.3061	1.0730	0.0868	0.0611
+1 EV/PQ (79MVA)	0.9625	0.3677	3.4328	1.2713	0.6725	0.0825

The results from Table 1 can be shown that the power loss, reactive loss and LVD from vary sizing of PQ load and EV load in to test system. To increase for sizing of EV load was increased the power loss reactive loss and load voltage deviation of power system more than PQ load. The LVD of system was shown each PQ load and EV load sizing to install in to at bus No.15. However, some sizing of PQ and EV load such as 20MVA can be improved load voltage deviation of power system. Therefore the EV load sizing had been effected total loss in power system and level of voltage deviation when compared with PQ load.

8. CONCLUSION

The modeling of EV load from development based on UDMs in PSAT programing can be used to solve power flow analysis. Therefore, the IEEE 14 bus test system can be used a very simple from GUI and quickly to solve the electrical power system problem from EV load model. In the results of test system show the sizing of EV load model were effected the steady state of voltage stability in term of voltage magnitude profile, total power loss, LVD and loading parameter. Future more, the studying location and sizing to install EV load in power system are necessary to optimize and suitable in the power system for system stability.

REFERENCES

[1]. C. H. Dharamakeerthi, N. Mithulananthan, and T. K. Saha, "Impact of electric vehicle fast charging on power system voltage stability", Electrical Power and Energy Systems, pp. 241-249., 2013.

[2]. C. H. Dharamakeerthi, N. Mithulananthan, and T. K. Saha, "Impact of Electric Vehicle Load on Power System Oscillatory Stability," Australasian Universities Power Engineering Conference, AUPEC 2013, Hobart, TAS, Australia, 29 September 2013.

[3]. A. Haidar and K. M. Muttaqi, "Behavioral characterization of electric vehicle charging loads in a distribution power grid through modeling of battery chargers," IEEE Transactions on Industry Application, Vol. 52, N0. 1, Jan/Feb 2016.

[4]. A. Jimenez and N. Garcia, "Power Flow Modeling and Analysis of Voltage Source Converter-Based Plug-in Electric Vehicles," IEEE Transactions on Power Systems, 2011.

[5]. R. Garcia-Valle and J. G. Vlachogiannis, "Letter to the Editor :Electric Vehicle Demand Model for Load Flow Studies", Electric Power Components and Systems, 37:577-582, 2009.

[6]. M. C. Kisacikonglu, B. Ozpinneci, and M. Leon, "EV/PHEV Bidirectional Charger Assessment for V2G Reactive Power Operation", IEEE Transactions on Power Electronics, Vol. 28, No. 12, Dec 2013.

[7]. H. Liu, H. Zhuang, and H. Wu, "Multi-Objective Dynamic Economic Dispatch of Migrogrid System Including Vehicle-to-Grid," Energies, 2015.

[8]. L. M. Hajagos and B. Danai, "Laboratory measurements and models of modern loads and Their effect on voltage stability studies," IEEE Transactions on Power Systems, Vol. 13, No. 2, May 1998.

[9]. J. Y. Yong, V. K. Ramachandaramurthy, K. Miao, and N. Mithulananthan, "Bi-directional electric vehicle fast charging station with novel reactive power compensation for voltage regulation," Electrical Power and Energy Systems, pp. 300-310, 2015.

[10]. C. H. Dharamakeerthi and N. Mithulananthan, "PEV load and its impact on static voltage stability," Plug In Electric Vehicles in Smart Grids Integration techniques, Chapter 8, pp.221-248

[11]. F. Milano, "An Open Source Power System Analysis Toolbox," IEEE Transaction on power systems, Mar 2005.

[12]. J. Koasungnean, Y. Kongjeen, P. Maksaen, and,K. Buayai, "Reconfiguration and capacitor placement for improve voltage quality and reduce power loss in primary distribution systems," Proceedings of the 7th Conference of Electrical Engineering Network of Rajamangala University of Technology, (EENET2015), 2015.

Single-carrier-based Pulsewidth Modulation Strategy for Grid-connected Three-level NPC Converter Based on Voltage Oriented Control

Watcharin Srirattanawichaikul, Suttichai Premrudeepreechacharn, Yuttana Kumsuwan, and **Dhanavich Chulikavit**

Manuscript received Aril 30, 2016
Revised June 5, 2016

ABSTRACT

This paper presents a modified carrier-based pulsewidth modulation (PWM) strategy for the grid-connected three-level neutral-point-clamped (NPC) converter system. The gating signals are generated by comparing the single carrier wave with the modified modulating waves. The control method of the grid-connected system is applied for the voltage oriented control scheme, which provides independent control active and reactive powers flow into the utility grid and maintain the dc-link voltage constant. The feasibility of the developed proposed modulation technique for the grid-connected three-level NPC converter system is confirmed by simulation and experiment results, which is validated the performance and effectiveness of the presented method.

Keywords: *Three-level neutral-point-clamped voltage source converter; carrier-based pulsewidth modulation technique; grid-connected system; grid-connected control strategy; multilevel converter.*

1. INTRODUCTION

Multilevel converter topologies have recently been extensively applied in high-power medium-voltage industrial applications. The advantages of these converters are higher quality output voltage waveforms, reduced output voltage and current harmonic distortions, and lower semiconductor voltage stress when compared with a standard two-level converter topology [1]. The most popular topology of multilevel converters is the three-level NPC converter. These converters play a pivotal role in high-power industrial applications such as composition of renewable energy sources, active-front-end converters for motor drive systems, grid-connected systems, and energy storage systems. Fig. 1 shows the equivalent circuit of the grid-connected three-level NPC converter. The control scheme of a grid-connected converter is usually providing control power factor, dc-link voltage regulation and low harmonic distortion of current [2]. Moreover, the modulation technique for three-level NPC converter should be designed the simple algorithm and processed very fast. Typically, the modulation technique for three-level NPC converter could be generally classified into two groups, which are carrier-based modulation technique and space vector modulation technique. Amongst these modulation techniques, the carrier-based modulation technique has probably been the most popular due to its simplicity of implementation.

Several modulation techniques have been found in recent literatures to the grid-connected three-level NPC converter applications. In [3] was presented a novel modulation strategy for a three-level NPC converter. The proposed modulation strategy is provided by adding the minimum and maximum of the reference voltages to the output reference voltages that is obtained from the modified modulation signals. The proposed modulation strategy completely removes the low-frequency voltage oscillations that appear in the neutral-point voltage. In addition, this technique can be implemented with a very simple algorithm and processed very fast. Nevertheless, this technique is required two triangular carriers with modulation signals for generate the gate pulses. The single-carrier modulation technique for three-level NPC inverter in photovoltaic (PV) systems was presented in [4]. This technique can eliminate the leakage current through the common-mode voltage control system. It has a very simple structure. Although this method performs well, it requires a specific and modified modulation switching signals with analog circuits. This increases the implementation cost and complexity of the method. The direct power control has been developed for PV grid-connected system with three-level NPC converter [5]. In this method, the active and reactive powers are used control variables. This method has demonstrated good dynamic performance of the grid-connected system.

Therefore, the main contribution of this paper is to present the superiority of modified modulation technique for the grid-connected three-level NPC converter system. This converter is operated on the voltage oriented control to maintain a dc-link voltage constant, and feed the active power into the utility grid. The paper is organized as follows. Section II gives configuration of the grid-connected three-level NPC

Watcharin Srirattanawichaikul, Suttichai Premrudeepreechacharn, Yuttana Kumsuwan, and Dhanavich Chulikavit are with the Department of Electrical Power Engineering, Faculty of Engineering, Chiang Mai University, Chiang Mai, Thailand(email:Watcharin@eng.cmu.ac.th, suttic@eng.cmu.ac.th,yt@eng.cmu.ac.th, dhanavich.ch@cmu.ac.th)

converter system. A voltage oriented control is used in this paper to control the grid-connected converter and the considerations required to implement the proposed modulation technique are discussed in Section III and IV, respectively. The simulation and experimental results which verify the proposed method are present in Section V. Finally, Section VI draws the conclusion.

2. CONFIGURATION OF THE GRID-CONNECTED THREE-LEVEL NPC CONVERTER SYSTEM

A. Description and Operation of Grid-connected Systems

Among the various multilevel converter topologies, the most popular topology in high power industrial applications is the three-level NPC converter. One of the advantages of this converter is that the power switches and the dc-link capacitors have to endure only one-half of the dc-link voltage. As a result, the converter can deal with double voltage and power value than in a standard two-level converter with the same switching frequency. Fig. 1 shows the simplified equivalent circuit of a grid-connected three-level NPC converter. The converter consists of twelve active switches and six anti-parallel diodes. The grid-side is connected using three inductors with loss resistor for inject current to cancel the harmonic component current. On the dc-link side of the converter, the dc-link voltage capacitor is split into two, providing a neutral point and must be regulated and balanced.

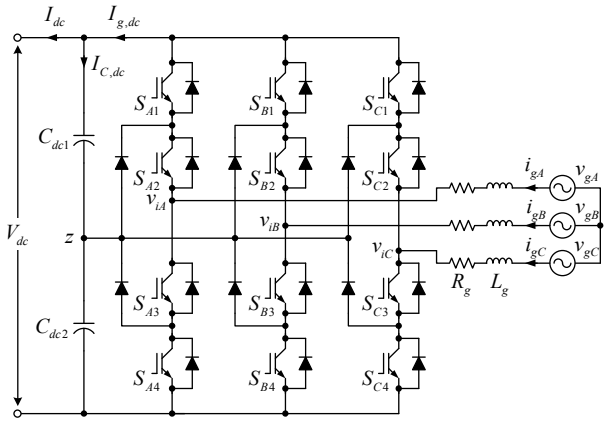

Fig.1. *Equaivalent circuit of the grid-connected three-level NPC converter.*

B. Dynamic Model of Grid-connected Systems

Considering the ac output from a converter in Fig. 1, assuming ideal commutation and neglecting the effect of harmonics, the voltage equations that model the grid-connected three-level NPC converter can be derived as follow:

$$\begin{cases} v_{gA} = R_g i_{gA} + L_g \dfrac{d}{dt} i_{gA} + v_{iA} \\ v_{gB} = R_g i_{gB} + L_g \dfrac{d}{dt} i_{gB} + v_{iB} \\ v_{gC} = R_g i_{gC} + L_g \dfrac{d}{dt} i_{gC} + v_{iC} \end{cases} \quad (1)$$

where v_{gA}, v_{gB}, v_{gC} are the phase grid voltages, v_{iA}, v_{iB}, v_{iC} are the phase grid-side converter voltages, i_{gA}, i_{gB}, i_{gC} are phase grid currents, R_g and L_g are the resistance and inductance of the utility grid.

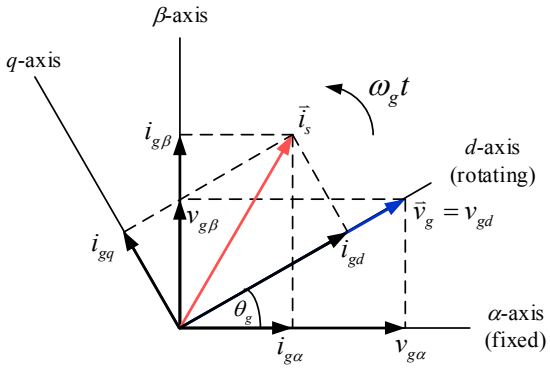

Fig. 2. *Phasor diagram of the grid-connected three-level NPC converter.*

A dynamic mathematical model of grid-side converter is developed in its original three-phase *abc* frame. This three-phase model is transformed into the *dq* rotating reference frame. From (1), the voltage equations of the grid-connected system on the rotating reference frame are depicted as follows:

$$\begin{cases} v_{gd} = R_g i_{gd} + L_g \dfrac{d}{dt} i_{gd} - \omega_g L_g i_{gq} + v_{id} \\ v_{gq} = R_g i_{gq} + L_g \dfrac{d}{dt} i_{gq} + \omega_g L_g i_{gd} + v_{iq} \end{cases} \quad (2)$$

where, v_{gd} and v_{gq} are the *d*-axis and *q*-axis grid voltages, v_{id} and v_{iq} are the *d*-axis and *q*-axis inverter voltages, i_{gd} and i_{gq} are the *d*-axis and *q*-axis grid currents, and ω_g is the electrical angular of the grid.

The phasor diagram for the vector control of the grid-connected converter is shown in Fig. 2. By placing the *d*-axis of the rotating reference frame on the utility grid voltage vector, v_{gq} and v_{gd} are set to zero and constant, respectively. The equations of the active power P_g and reactive power Q_g in rotating reference frame, which is aligned in the utility grid, can be calculated as

$$\begin{cases} P_g = 1.5 v_{gd} i_{gd} \\ Q_g = -1.5 v_{gd} i_{gq} \end{cases} \quad (3)$$

From eq. (3), the grid-connected control system can be produced active and reactive powers with the controlled *d-q* axis current components. The *q*-axis current component is set to variable for reactive power control. The dc power has to be equal to the active power flowing between the utility grid and the dc-link converter. Thus,

$$C_{dc}\frac{d}{dt}V_{dc} = I_{C,dc} = I_{g,dc} - I_{dc} \tag{4}$$

where V_{dc} is the dc-link voltage, I_{dc} is the current between the dc-link and the rotor-side converter, $I_{g,dc}$ is the current between the dc-link and the grid-side converter, and C_{dc} is the dc-link capacitor.

3. CONTROL SYSTEM OF GRID-CONNECTED THREE-LEVEL NPC CONVERTERS

To illustrate the control system of the voltage oriented control method for the grid-connected three-level NPC converter system is presented in this section. The purpose of the grid-connected system is to present the modified modulation technique in generated the gating signals for the grid-connected three-level NPC converter system as shown in Fig. 3. The three-level NPC converter is operated on the voltage oriented control to maintain a dc-link voltage constant, and feed the active power into the utility grid. Traditionally, the grid-connected converter can be used to produce active and reactive powers with the controlled *d-q* axis current components, respectively.

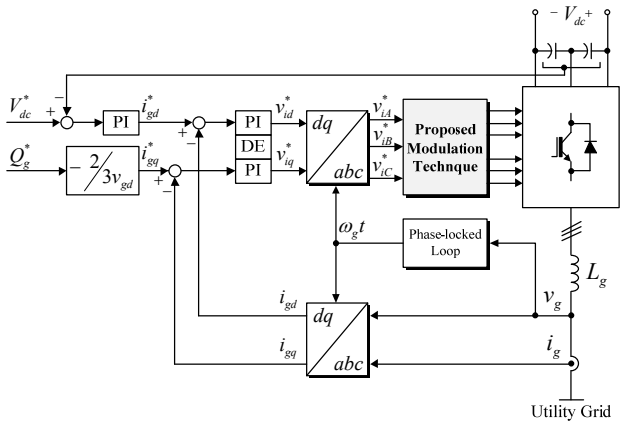

Fig. 3. *Block diagram of the proposed grid-connected three-level NPC converter system and controller using the proposed modulation technique.*

For the grid-connected voltage oriented control, a complete control scheme of the grid-connected three-level NPC converter is indicated in Fig. 3. This scheme has three control loops, one external loop to control the dc-link voltage and two internal loops to regulate the *d-q* current components, the *d*-axis current component is utilized to regulate the dc-link voltage and the *q*-axis current component is utilized to control the reactive power. The output active power and the power factor of the utility grid can be controlled by changing *d*- and *q*-axis current components, respectively.

In the control scheme, the dc-link voltage controller is the outer loop, while the current controller is the inner loop. The main objective of the control scheme is to regulate dc-link voltage V_{dc} to follow the reference value V_{dc}^*, while the grid current is sinusoidal shape and either in-phase or out of phase with the utility grid. The dc-link voltage error is delivered to proportional-integral (PI) dc-link voltage controller, which generates the reference value of the current in *d*-axis component i_{gd}^*. To achieve the unity power factor condition in the grid-side converter, the referenced current value of *q*-axis component i_{gq}^* is set to zero, $Q_g^* = 0$ VAR.

The current errors are delivered to PI current controllers that generate the inverter voltage references. The compensations correspond to the inverter voltage references and decoupling terms (DE) of the current components. Therefore, the inverter voltage references v_{id}^*, v_{iq}^* can be given by:

$$\begin{cases} v_{id}^* = v_{Lgd}^* + \omega_g L_g i_{gq} + v_{gd} \\ v_{iq}^* = v_{Lgq}^* - \omega_g L_g i_{gd} \end{cases} \tag{5}$$

After transformation into the three-phase reference frame, the reference voltage $v_{iA}^*, v_{iB}^*, v_{iC}^*$ are delivered to the proposed modulation technique which generates switching signals for the three-level NPC converter.

H. Design of dc-link voltage control

The dc-link voltage controller is used to generate the reference current in *d*-axis component for the current controller. The aim of this controller is to keep the dc voltage constant on the dc-link, which is changed according to balance of power replaced by the converter. The design of the dc-link voltage controller has been designed to achieve short settling time and fast correction of the error. The dc power has to be equal to the active power, $P_{dc} = P_g$, flowing between the utility grid and the dc-link inverter. The expression for the average dc-link grid-side current $I_{g,dc}$ is given by

$$I_{g,dc} = \frac{3}{2}\frac{v_{gd} i_{gd}}{V_{dc}} \tag{6}$$

Substituting (6) into (4), the differential equation of the dc-link voltage is expressed as

$$\frac{d}{dt}V_{dc} = \frac{3}{2}\frac{v_{gd} i_{gd}}{V_{dc} C_{dc}} - I_{dc} \tag{7}$$

By Laplace transform in (7), the closed-loop transfer function of the dc-link voltage controller, obtained from Fig. 4, can be written as

$$\frac{V_{dc}(s)}{V_{dc}^*(s)} = \frac{\frac{3}{2}\frac{V_{gd}}{V_{dc}C_{dc}}\left(k_{pv}s + k_{iv}\right)}{s^2 + \frac{3}{2}\frac{V_{gd}}{V_{dc}C_{dc}}k_{pv}s + \frac{3}{2}\frac{V_{gd}}{V_{dc}C_{dc}}k_{iv}} \tag{8}$$

Therefore, the parameters of PI controller of dc-link voltage control can be calculated as

$$\begin{cases} k_{pv} = \dfrac{2}{3}\dfrac{V_{dc}}{V_{gd}} 2\xi\omega_{nv} C_{dc} \\ k_{iv} = \dfrac{2}{3}\dfrac{V_{dc}}{V_{gd}} \omega_{nv}^2 C_{dc}. \end{cases} \tag{9}$$

where k_{pv} and k_{iv} are the proportional and integral parameters of the dc-link voltage control, respectively, ω_{nv} is the natural angular frequency of dc-link voltage control, and ξ is the damping ratio.

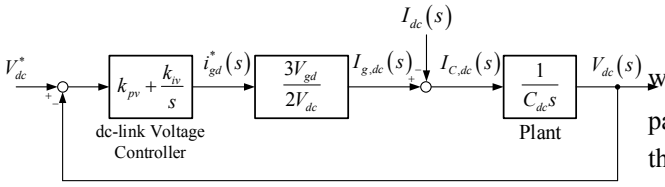

Fig. 4. *Block diagram of the dc-link voltage control.*

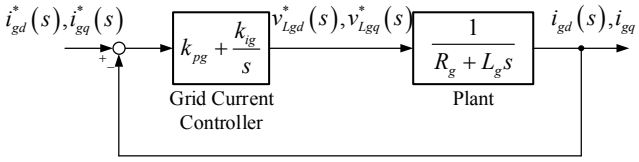

Fig. 5. *Block diagram of the grid current control.*

I. Design of grid-connected current control

The *d*-axis and *q*-axis current controllers have the same dynamic controls. Considering (2) with the *d*-axis of rotating reference frame aligned to the utility grid voltage vector, the grid-side inductance voltage references v_{Lgd}^*, v_{Lgq}^* are specified as

$$\begin{cases} v_{Lgd}^* = R_g i_{gd} + L_g \dfrac{d}{dt} i_{gd} \\ v_{Lgq}^* = R_g i_{gq} + L_g \dfrac{d}{dt} i_{gq} \end{cases} \tag{10}$$

By Laplace transform the voltage equations in (10), the transfer function of the grid current loop can be written as

$$\frac{i_{gd}(s)}{v_{Lgd}^*(s)} = \frac{i_{gq}(s)}{v_{Lgq}^*(s)} = \frac{1}{R_g + L_g S} \tag{11}$$

Equation (11) shows that the relationship between grid-side current and the grid inductance voltage is equivalent to a first order system, which is suitable for both *dq* current loops. The PI controller for achieving good performance of tracking the *dq* reference current signals can be synthesized for the desired closed-loop transfer function. Therefore, the closed-loop transfer function of the current controller in Fig. 5 can be written as

$$\frac{i_{gd}^*(s)}{i_{gd}(s)} = \frac{i_{gq}^*(s)}{i_{gq}(s)} = \frac{\dfrac{k_{pi}s + k_{ii}}{L_g}}{s^2 + \dfrac{R_g + k_{pi}}{L_g} s + \dfrac{k_{ii}}{L_g}} \tag{12}$$

From the general form of the characteristic equation in (12), the parameters of PI controller of grid current control can be calculated as

$$\begin{cases} k_{pi} = 2\xi\omega_{ni} L_g - R_g \\ k_{ii} = \omega_{ni}^2 L_g \end{cases} \tag{13}$$

where k_{pi} and k_{ii} are the proportional and integral parameters of the grid control, respectively, and ω_{ni} is the natural angular frequency of grid current control.

4. PROPOSED PULSEWIDTH MODULATION STRETAGY FOR THREE-LEVEL NPC CONVERTER

The traditional carrier-based modulation technique of the three-level NPC converter uses the sinusoidal/non-sinusoidal modulation techniques, which compared with two triangular carrier signals [6]. The three-phase sinusoidal reference signals $v_{A,B,C}^*$ can be given by

$$\begin{cases} v_A^* = m_a \cos(\omega_s t) \\ v_B^* = m_a \cos(\omega_s t - 2/3\pi) \\ v_C^* = m_a \cos(\omega_s t + 2/3\pi) \end{cases} \tag{14}$$

where m_a is the modulation index and $\omega_s t$ is the phase angle (ω_s is the angular frequency, $2\pi f_s$).

The proposed modulation technique is modified the sinusoidal modulating signal that uses the effective three-phase sinusoidal reference signal and the maximum and minimum of the three reference signals. This technique is based on only single triangular carrier signal for generated the gating pulses to the three-level converter. The general form of the modified modulation reference signal equation for the proposed modulation technique is defined as

$$\begin{cases} v_{AM}^* = v_{AP}^* + v_{AN}^* \\ v_{BM}^* = v_{BP}^* + v_{BN}^* \\ v_{CM}^* = v_{CP}^* + v_{CN}^* \end{cases} \tag{15}$$

where $v_{ABC,M}^*$ is the modified modulation reference signals and $v_{ABC,P}^*, v_{ABC,N}^*$ are the positive and negative reference signals.

The positive reference signals take the minimum of the three-reference signals and subtract this value from each of the three-phase sinusoidal reference signals, which can be expressed as,

$$\begin{cases} v_{AP}^{*} = \dfrac{v_A^{*} - \min\left(v_A^{*}, v_B^{*}, v_C^{*}\right)}{2} \\ v_{BP}^{*} = \dfrac{v_B^{*} - \min\left(v_A^{*}, v_B^{*}, v_C^{*}\right)}{2} \\ v_{CP}^{*} = \dfrac{v_C^{*} - \min\left(v_A^{*}, v_B^{*}, v_C^{*}\right)}{2} \end{cases} \quad (16)$$

Similar to (16), the negative reference signals take the maximum of the three-reference voltages and subtract this value from each of the three-phase sinusoidal reference signals,

$$\begin{cases} v_{AN}^{*} = \dfrac{v_A^{*} - \max\left(v_A^{*}, v_B^{*}, v_C^{*}\right)}{2} + 1 \\ v_{BN}^{*} = \dfrac{v_B^{*} - \max\left(v_A^{*}, v_B^{*}, v_C^{*}\right)}{2} + 1 \\ v_{CN}^{*} = \dfrac{v_C^{*} - \max\left(v_A^{*}, v_B^{*}, v_C^{*}\right)}{2} + 1 \end{cases} \quad (17)$$

The proposed modulation technique is shown in block diagram of Fig. 6, where the three-phase sinusoidal reference signals v_{ABC}^{*} to generate the modified modulation reference signals $v_{ABC,P}^{*}, v_{ABC,N}^{*}$. It can be seen that the modified modulation reference signals are compared with the single triangular carrier signal to generate the logic 0 or 1 signals of the $S_{A,1-4}, S_{B,1-4}, S_{C,1-4}$. The logic of gate pulses is very simple as follows: if $v_{ABC,P}^{*} \geq v_{tri} \Rightarrow S_{ABC,1} = \text{ON},\ S_{ABC,3} = \text{OFF}$ and if $v_{ABC,N}^{*} \geq v_{tri} \Rightarrow S_{ABC,2} = \text{ON},\ S_{ABC,4} = \text{OFF}$. Since the inner gating pulses $S_{ABC,3}$ operate complementary with $S_{ABC,1}$ and $S_{ABC,4}$ operate complementary with $S_{ABC,2}$. The practical implementation method is proposed modulation technique using offset reference signal concept. The main point of the proposed technique is used only single triangular carrier signals for generated the specified gating signals for three-level NPC converter.

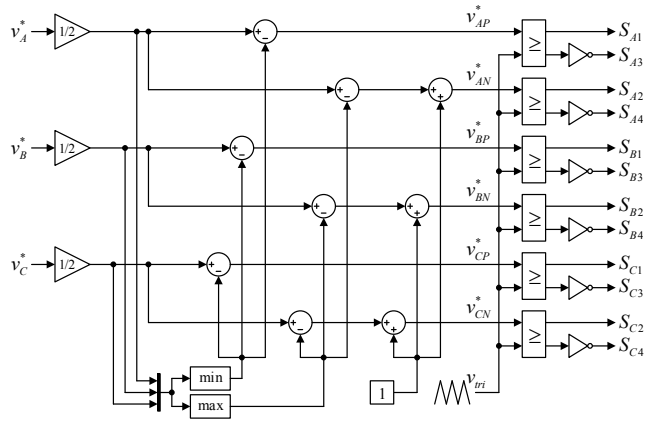

Fig. 6. *Block diagram of the proposed modulation technique for three-level NPC converter.*

5. SIMULATION AND EXPERIMENTAL RESULTS

In this section, simulation and experimental system was built, and various results are presented. To evaluate the performance of the proposed system, simulations are performed by using Matlab/Simulink software. The operation of grid-connected three-level NPC converter is experimented to evaluate the proposed modulation technique, which is represented by the block diagram as shown in Fig. 7. The three-level NPC converter prototype is realized using SEMIKRON SKM50GB123D IGBT modules and SEMIKRON SKKD42F12 diode modules. Each leg of converter is equipped with the two switch IGBT modules and the single clamped diode module. A three-level NPC converter is connected to utility grid with the 380V, 50Hz through the three-phase transformer (turn ratio 1:4). A dc power supply rated at 5kW is connected to the dc-link. The nominal converter dc-link voltage is controlled at 180 V, the switching frequency of the converter is 2.5 kHz, the dc-link capacitors are 3,300 μF each, and the low-pass filter of grid is 12 mH. The proposed control method is implemented in a ds1104 real-time control board, which acquires the dc and ac voltages and currents. The digital platform sends the gate signals directly to the gate driver circuit of the three-level NPC converter.

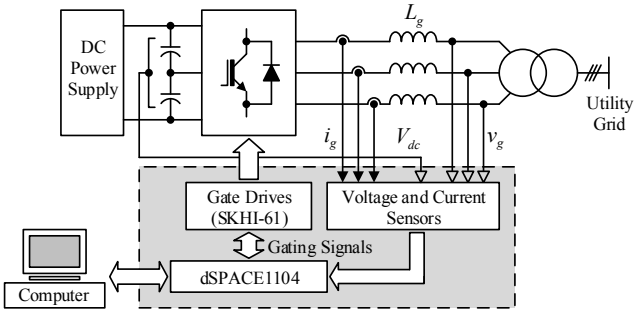

Fig. 7. *Configulation of the experimental set-up.*

J. Simulation results

The simulated design is carried out to verify the validity of the proposed system. The modified modulating signals of the proposed technique are given in Fig 8. In Fig. 8 (top), the sinusoidal modulating signals $v_A^{*}, v_B^{*}, v_C^{*}$ are used to generate the modified modulating signals as shown in Fig. 8 (middle). From these figures, it can be shown that the waveforms of the modified modulating signals are compared with the single triangular carrier signal where the amplitude of the modulation index is defined as the relation between the peak amplitude of triangular carrier signal. The modulated gating signals can be generated using proposed the modulation technique for three-level NPC converter as shown in Fig. 8 (bottom).

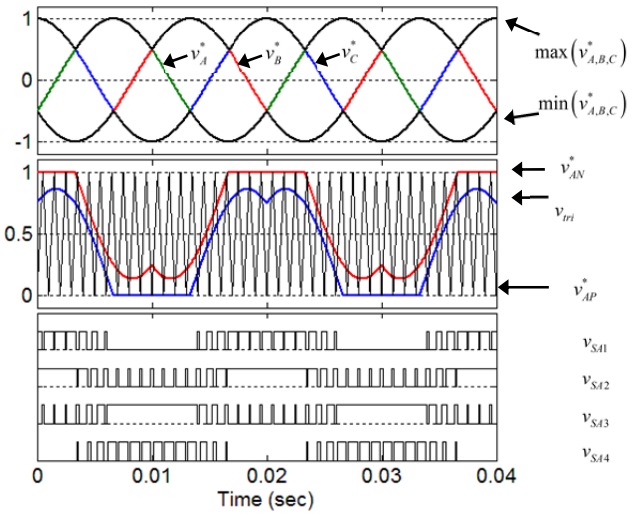

Fig. 8. *Single triangular carrier-based modulation technqiue for generating gate signals.*

Fig. 9 (a) also shows voltage and current waveforms of the converter operating in the inverting mode. In this condition, the active power flows from the dc-link side into the utility grid. The phase displacement between the grid-connected phase grid voltage and current of converter is out of phase and the dc-link voltage is kept constant. Similarly, Fig. 9 (b) shows the simulated waveform by the converter for operation in the rectifying mode. In this mode, the active power flows into the dc-link, with in phase displacement between the grid-connected grid voltage and the grid current.

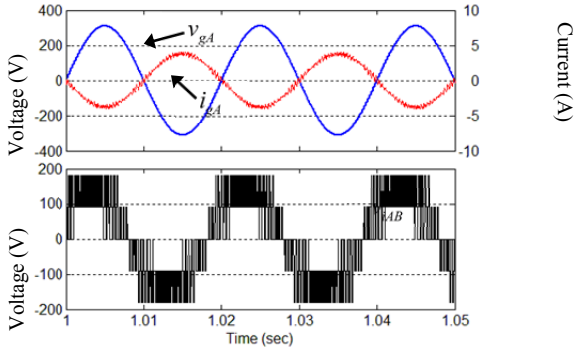

(a)

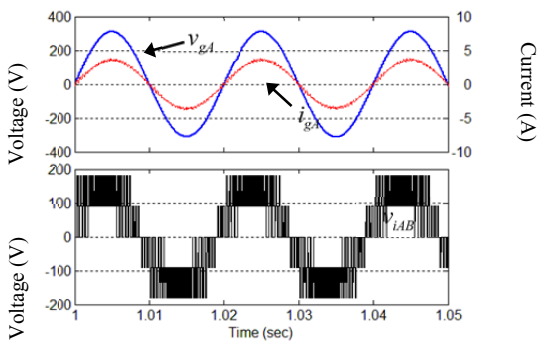

(b)

Fig. 9. *Simulation results of the proposed modulation technique for grid-connected three-level NPC converter in unity power factor operation. (a) Inverting mode. (b) Rectifying mode.*

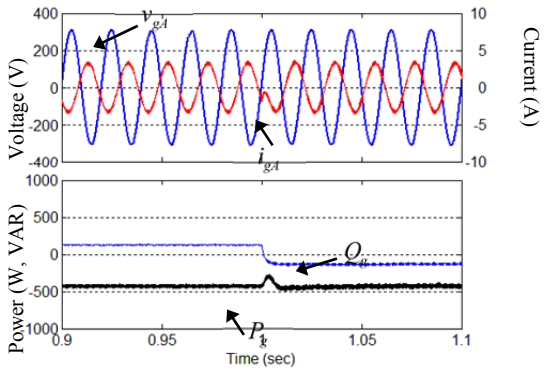

Fig. 10. *Simulation results of the proposed modulation technique for grid-connected three-level NPC converter of dynamic respone operation in the inverting mode.*

As discussed earlier, the power factor of the system can be controlled by adjusting the reference of the reactive power. As can be seen from Fig. 10, the dynamic response of the converter to a step changed in reactive power reference control with active power flowing from the dc-link into the grid. The reactive power is stepped from +120 VAR to -120 VAR and the active power is kept constant. It can be seen that the grid current of converter can operate under the leading and lagging power factor condition with the performance of the dc-link voltage constant.

K. Experimental results

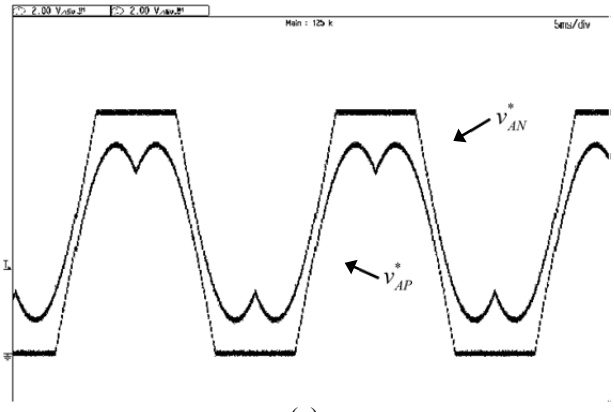

(a)

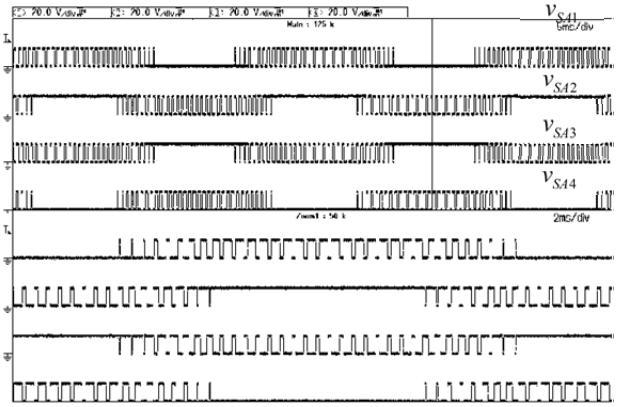

(b)

Fig. 11. *Experimental results of the proposed modulation technique in phase A. (a) Modulation reference signals. (b) Gating signals.*

The experimental results of the proposed prototype-based laboratory prototype have been presented to demonstrate the proposed system in practice as shown in Figs. 11 and 13. Fig. 11 (a) and (b) show measured waveforms of the proposed modified reference signals and gating signals for power switches in phase *A* at the modulation index of 0.8. The references can share single triangular carrier signal. Therefore, the modulation signals for the power switches located in phase *B* and *C* can be obtained by $\pm 120^{\circ}$ phase-shifting, respectively.

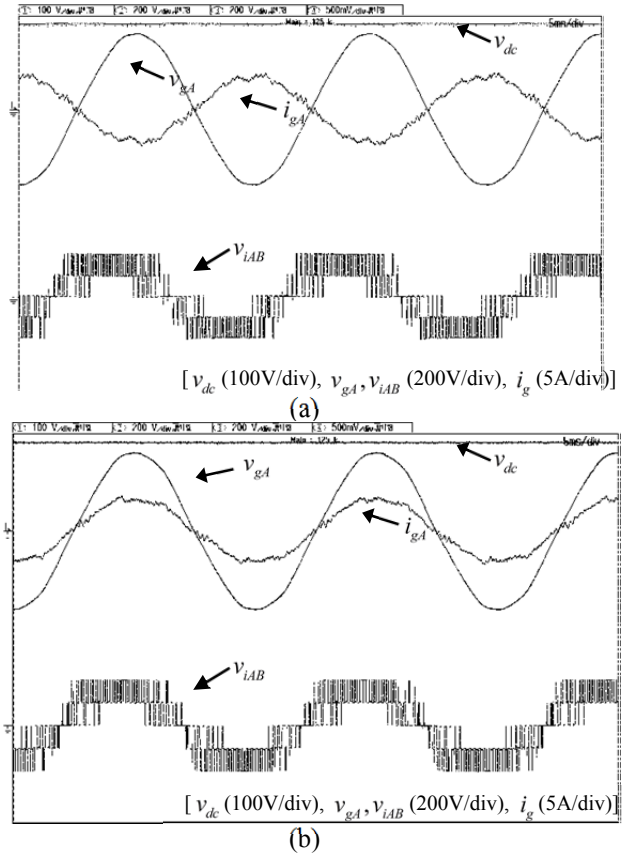

Fig. 12. *Experimental results of the proposed modulation technique for grid-connected three-level NPC converter in unity power factor operation. (a) Inverting mode. (b) Rectifying mode.*

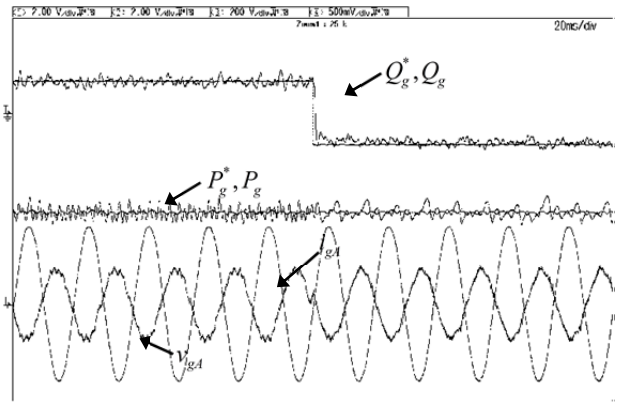

Fig. 13. *Experimental results of the proposed modulation technique for grid-connected three-level NPC converter of dynamic respone operation in the inverting mode.*

Fig. 12 (a) shows dc-link voltage v_{dc}, the grid phase voltage v_{gA} and the current i_{gA} in phase *A*, and the line-to-line voltage of the three-level NPC converter v_{iAB} at unity power factor operation. In this condition, the active power flows from the dc-link into the utility grid. The reference of the reactive power Q_g^* is controlled to zero. It can be seen that the grid phase current is out of phase with the grid phase voltage. It guarantees a null reactive power on the utility grid. Similarly, Fig. 12 (b) also shows experimented waveforms in the rectifying mode. In this operation mode, the active power flows into the dc-link, with in phase displacement between the grid-connected grid voltage and the grid current.

The dynamic response of the voltage oriented control technique to a step change in the reactive power reference with active power flowing from the dc-link into the utility grid is shown in Fig. 13. The reactive power reference is step changed from -120 to +120 VAR and the active power is kept constant at -420 W. It can be seen that the grid-side converter can operate under the leading and lagging power factor condition with keeping the dc-link voltage constant. There are not overshoot of either the grid current or the active and reactive powers.

6. CONCLUSION

This paper proposes a modulation strategy for the grid-connected three-level NPC converter system. The proposed technique is employed only single triangular carrier signal for generated the gating signals in the converter and significantly simplifies the modulation technique. The advantages are simple modulation algorithm, reduced capacitor voltage ripple, lower switching frequencies, and easy hardware implementation. This paper has also proposed the control method of voltage oriented control for the grid-connected system. The objective of the grid-side converter control is to maintain the dc-link voltage and independently control active and reactive power flow. The experimental result confirms that proposed technique is able to achieve good dynamic responses and high accuracy in active and reactive power controls.

ACKNOWLEDGMENT

The authors would like to thank the Faculty of Engineering, Chiang Mai University.

REFERENCES

[1]. J. Rodríguez, J. Lai, and F. Peng, "Multilevel inverters: A survey of topologies, controls and applications," *IEEE Trans. Ind. Electron.*, vol. 49, no. 4, pp. 724-738, Aug. 2002.

[2]. F. Blaabjerg, R. Teodorescu, M. Liserre, and A. V. Timbus, "Overview of control and grid synchronization for distributed power generation systems," *IEEE Trans. Ind. Electron.*, vol. 53, no. 5, pp. 1398–1409, Oct. 2006.

[3]. J. Pou, J. Zaragoza, P. Rodriguez, S. Ceballos, V. M. Sala, R. P. Burgos, and D. Boroyevich, "Fast-Processing Modulation Strategy for the Neutral-Point-Clamped Converter with Total Elimination of Low-Frequency Voltage Oscillations in the

Neutral Point," IEEE Trans. Ind. Electron., vol. 54, no. 4, pp. 2288–2294, Aug. 2007.

[4]. X. Guo, M. C. Cavalcanti, A. M. Farias, and J. M. Guerrero, "Single-carrier modulation for neutral-point-clamped inverters in three-phase transformerless photovoltaic systems," *IEEE Trans. Power Electron.*, vol. 28, no. 6, pp. 2635-2637, June 2013.

[5]. J. A. Martinez, J. E. Garcia, and S. Arnaltes, "Direct power control of grid connected PV systems with three-level NPC converter," *Solar Energy*, vol. 84, pp. 1175-1186, 2010.

[6]. R. M. Tallam, R. Naik, and T. A. Nondahl, "A carrierbased PWM scheme for neutral-point voltage balancing in three-level inverters," *IEEE Trans. Ind. Appl.*, vol. 41, no. 6, pp. 1734-1743, Nov./Dec. 200

Factors Determining towards the Rate of Adoption of Voice over LTE (VoLTE)

Chalermwutt Ratchakhom and Arnon Tubtiang

Manuscript received May 10, 2016
Revised June 17, 2016

ABSTRACT

The main purpose of this research were study the factors determining towards the rate of adoption of Voice over LTE (VoLTE), a case study of a telecommuni-cation operator. The researcher employed Adoption of Innovation theory (Everett M. Rogers, 2003). The subjects were 400 employees of a telecommunication operator in Thailand who were selected by accidental sampling. The research revealed that (1) Demographic factors including gender, age, education, work experience were not determining towards the rate of adoption of VoLTE (2) Factors determining towards the rate of adoption of VoLTE were perceived attributes of innovations (including relative advantage, compatibility, complexity, trainability, and observability), communica- tion channels, nature of the social systems, extent of change agents' promotion efforts.

Keywords: *Engineering Management, Forth Generation, Voice over LTE, Long Term Evaluation*

1. INTRODUCTION

Nowadays, communication is somewhat important to life and business. Telecommunication industry is the key driven world economic. Products and services provider apply functional of mobile technology to generate new products and services [1]. Through the convenience of portability to use anywhere, the mobile phone becomes the essential gadget to be the personal entertainments or business transactions [2].

When looking backward to 2010, the total number of mobile subscriptions was around 7.3 billion, including 539 million subscription for smartphones, but currently, the number of smartphone subscriptions is noticeably growing. The total number of mobile subscriptions in November 2015 was 3,352 million and approximately 3,958 million in 2016. By 2016 the number of smartphone subscriptions will surpass those for basic phones [3].

Chalermwutt Ratchakhom and Arnon Tubtiang are with Graduate School of Management and Innovation, King Mongkut's University of Technology, 126 CB5 8th Floor, Pracha-Utid Road, Bangmod, Thungkru, Bangkok 10120
arnon.tub@kmutt.ac.th

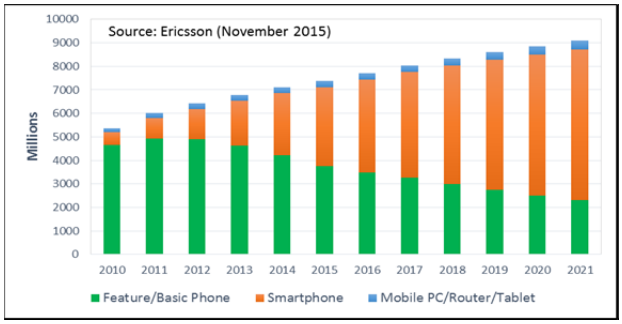

Fig. 1 *The forecast of number of mobile subscriptions, split per device types. (Source: Ericsson 2015)*

Mobile broadband has created opportunities and opened up new revenue streams for mobile operators. Opportunities are often coupled with challenges, and mobile broadband tests the position of communication services, such as voice, which today account for around 60 percent of operators' annual revenue or about USD 600 billion in 2014, globally. The precious question is how to take advantage of mobile broadband opportunities, while maintaining and increasing revenues from communication services for consumers as well as for business users at the same time [4].

LTE networks can deliver mobile broadband with greater data capacity and lower latency. However, as there is no circuit-switched voice domain in LTE, the mobile industry has adopted a globally interoperable IP-based voice and video calling solution for LTE, known as VoLTE, which also enables development of new innovative communication services.

GSMA reported, commercially VoLTE services were launched in 51 mobile network operators in 29 countries globally by 29 February 2016 [5].

For Thailand, The Thailand Telecommunications Indicators Year 2014-2015 reported, there are 97.1 million mobile subscriptions or 144.91 mobile subscription a hundred of population and increasing approximately 121.02 million by 2019 [6].

Table 1 *The Thailand Telecommunications Indicators Year 2014-2015*

	Mobile	
	2014	2015(f)
Mobile subscriptions (million)	97.10	83.05
A hundred populations	144.91%	123.53%

Source: NBTC, 2015

2. MATERIALS AND METHODS

2.1 Concept of Voice over LTE (VoLTE)

Natively speech service on cellular network was sending voice through circuit-switched. Although, data services were supported since second-generation (2G) of mobile systems were introduced in the end of 1980s, but on 2G/3G mobile systems, voice and data channel were separated [7],[8]. Fourth-generation (4G) was introduced without voice channel, only package-switched was developed, so while we are using data services on 4G, mobile phone will be switching to using voice channels on 2G/3G if voice services was originating or terminated.

Voice over LTE technology was developed for decoding speech into Internet Protocol (IP), then deliver though LTE network. With this solution we can use speech services on LTE networks [7],[8]. VoLTE has become an evolution of Fourth Generation (4G) which is based on the IP Multimedia Subsystem (IMS) network. This approach results in the voice services (control and media planes) were delivered as data flows within the LTE data bearer. This means that there is no dependency on the legacy circuit-switched voice network to be maintained.

2.2 Theory and Concept of Innovation Adoption

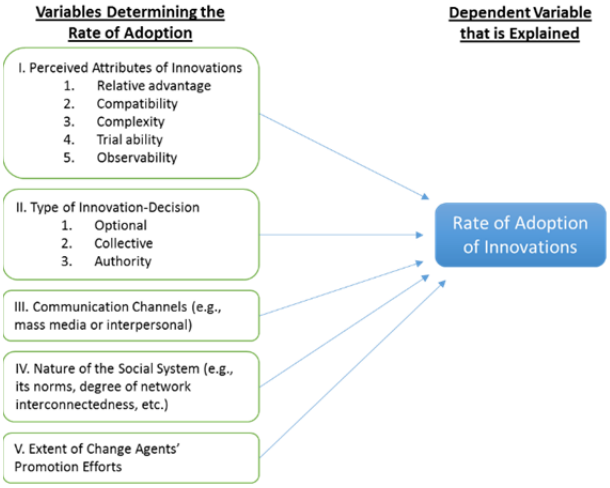

Fig. 2 *The forecast of number of mobile subscriptions, split per device types. (Source: Rogers (2003))*

Rate of adoption is generally measured as the number of individuals who adopt a new idea. There were five factors that determine rate of adoption of an innovation [8].

2.2.1 The perceived attributes of an innovation.

The most five attributes are explaining the most of the variance including [9],[10]: 1) relative advantage, such as how does the new idea benefits over old ides, 2) compatibility, such as how does the new idea consistent with individual routine, 3) complexity, such as how easy to learn on the new idea, 4) trainability, such as how can demo the new idea, 5) observability, such as how can experienced from adopted.

2.2.2 Type of Innovation-Decision

Innovations which was adopted by organization with authority or collective decision making are generally adopted more rapidly than when an innovation is adopted by individual-optional [9].

2.2.3 Communication Channels

Variety and diversity of communication channels help to delivering the information of new idea to adopters becomes awareness of innovation [9].

2.2.4 Nature of Social Systems

A new idea which was introduced in the social systems which high earlier adopters will be high rate of innovation-adoption [9].

2.2.5 Extent of Change Agents' Promotion Efforts

In this study mean telecommunication operators who put effort introducing the innovation to adopters to aware the benefit and compatibility to their life [9].

2.3 Research Model and Hypotheses

According to the theory, this study has in total 5 hypotheses as the follows:-

H1: The perceived attributes of VoLTE in adopters view affects adoption of VoLTE.

H2: Type of innovation-decision affects adoption of VoLTE.

H3: Communication channels affects adoption of VoLTE.

H4: Nature of social systems affect adoption of VoLTE.

H5: Extent of change agents' promotion efforts affects adoption of VoLTE.

In additional to these five variables, researcher was including additional two factors were:-

H6: Difference demography attributes is difference rate of adoption of VoLTE.

H7: The influence of substitution technology affect adoption of VoLTE.

Correspondingly, totally seven hypotheses have been assumed.

3. RESULTS AND DISCUSSION

Table 2 *The difference of demography on VoLTE adoption attitude.*

	Sex	Age	Education	Work Experience
VoLTE's rate of Adoption	✖	✖	✖	✖

✓ Difference with significant level at 0.05.

✖ Not difference with significant level at 0.05.

In this study, ordinal and nominal measure was developed to test the difference of demography attributes and type of innovation-decision.

Table 2 shows that there are not different adoption attitude to adopt VoLTE measured by group of demography attributes including, sex, age, education, working experience.

Also for measured by group of type of innovation-decision on VoLTE adoption attitude shown in table 3.

Table 3 *The difference of Type of Innovation-Decision on VoLTE adoption attitude.*

	Type of Innovation-Decision
VoLTE's rate of Adoption	✖

✓ Difference with significant level at 0.05.

✖ Not difference with significant level at 0.05.

Others factors measured by using scale measure, the questionnaire was reviewed by four specialists and tested index of item objective congruence before 40 set of questionnaire were used to test reliability of all questions by Cronbach's Alpha Coefficient scale.

Table 4 shows outcome of the reliability test that all variables where consistent and reliable to be applied as research instrument in this study with Cronbach's Alpha greater than 0.7

Table 4 *Summary of Reliability Analysis.*

Variables	**Cronbach's alpha**
Perceived Attributes of Innovations	0.778
Communication Channels	0.789
Nature of the Social Systems	0.798
Extent of Change Agents' Promotion Efforts	0.893
Substitution Technology and Services	0.754

Based on the result of table 5, found the Adjusted R Square was 0.203, represent to the percentage of variance can be explained by five factors which was 20.3 percent for adoption of VoLTE.

Table 5 *Result of model summary for the factor determining towards the rate of adoption of Voice over LTE (VoLTE)*

Model	**Adjusted R Square**
1	0.203

It was found that significance value of perceived attributes of VoLTE, communication channels and nature of social systems, change agents' effort are less than significant level at 0.05, while significance value the influence of substitution technology greater than significant level at 0.05. Therefore, H1, H3, H4, H5 are supported, except H7. It means that perceived attributes of VoLTE, communication channels and nature of social systems, change agents' effort are affecting on VoLTE adoption where the regression equation is

ADOPT = 1.851 + 0.255 (PE) + 0.118 (COMM) + 0.082 (SO) + 0.261 (OPER),

where:

ADOPT is VoLTE adoption,
PE is perceived attributes of VoLTE,
COMM is communication channels,
SO is nature of social system, and
OPER is change agents' efforts.

Table 6 *Result of Multiple Regression Analysis.*

Variables	**Unstandardized Coefficients (B)**	**Standardized Coefficients (Beta)**	**Sig.**
Constant	1.851		0.000
Perceived attributes of VoLTE	0.255	0.196	0.000
Communication Channels	0.118	0.145	0.002
Nature of Social Systems	0.082	0.098	0.036
Change Agents' Effort	0.261	0.273	0.000
Substitution Technology	-0.052	-0.057	0.205

The regression results revealed that coefficient represented by perceived attributes of VoLTE is 0.255, so every unit increase in perceived attributes of VoLTE, a 0.225 unit increase in VoLTE adoption is predicted. Coefficient of communication channels is 0.118. It means that every unit increase in communication channels, a 0.118 unit increase in VoLTE adoption is predicted. 0.082 is coefficient represented by nature of social systems. It means that every unit increase in nature of social systems, researcher expects a 0.082 increase in VoLTE adoption. For change agents' efforts, the coefficient is 0.261, so every unit increase in change agents' efforts, a 0.261 unit increase of VoLTE adoption is predicted. Furthermore, the change agents' efforts with largest beta coefficient is most significant independent variable follow by perceived attributes of VoLTE, communication channels and nature of social systems.

Table 7 shows that the result of examination of tolerance and VIF for independent variable are perceived attributes of VoLTE, communication

channels, nature of social systems, change agents' effort, substitution technology which tolerances are greater than 0.1 and approach to 1.0 and VIFs are less than 10.0. Therefore, multicollinearity is not found in this analysis.

Table 7 *Result of Multiple Collinearity Analysis*

Variables	Collinearity Statistics	
	Tolerance	VIF
Perceived attributes of VoLTE	0.911	1.098
Communication Channels	0.927	1.079
Nature of Social Systems	0.917	1.091
Change Agents' Effort	0.906	1.104
Substitution Technology	0.986	1.014

4. RECOMENDATIONS

Regarding to the study result, the result reveals the change agents' promotion efforts (or in this study represent to telecommunication operators) is the most important factor that affect the users' VoLTE adoption follow by perceived attributes of VoLTE, such as: relative advantage, compatibility, complexity, trainability, observability. It mean telecommunication operators shall put effort to show to adopters, how VoLTE benefits them over traditional voice services. Based on regression equation more promotion efforts, more perceived attributes of VoLTE will get more adoption. Also, the social systems which high early adopters and media communicational advances, adopters will be easier aware and adopt. Moreover, as summary in this research found the influence of substitution technology was not affects VoLTE adoption. By observing, VoLTE services is native function bundled into handsets whatever adopters want or not.

However, this research as limitations in geographic areas because VoLTE services are not commercially launch in nation-wide. So researcher sampling the data from employee of a telecommunication operator in Thailand. Who known the service functions and get in touch with new technology. For the future study, other researchers should collect the data from differences sampling groups both from technological employees and other occupations in order to get into the depth of study because difference occupations will have difference life styles and thinking. As the values of adjusted R square (0.203) this show that there are further variables around 79.7% more than the variables provided in this study which may affect VoLTE adoption.

5. CONCLUSIONS

In this study, the result reveals several factors determining towards the VoLTE adoption in Thailand. VoLTE has become an evolution of Fourth Generation (4G) which is based on the IP Multimedia Subsystem (IMS) network. This approach results in the voice services (control and media planes) being delivered as data flows within the LTE data bearer. In order to increase rate of VoLTE adoption, change agents' promotion efforts (0.261) is most encouraged. Also perceived attributes of VoLTE (0.255), communication channel (0.118), nature of social systems (0.082) are considered. In the hypothesis testing, hypothesis one, three, four, five, seven were analyzed to explore the direction of variables by using Pearson Correlation. Moreover, examine the factor affecting the VoLTE adoption by using multiple regression analysis. Other, hypothesis two and six were analyzed by using T-Test and One-way Anova to explore how difference on VoLTE adoption attitude by attribute of each. All data sampling from employee of a telecommunication operator who known the service functions and get in touch with this new technology in Thailand. Base on the result from hypothesis two and six, type of innovation-decision, demography attributes: sex, age, education, working experience, were not different attitude on VoLTE adoption. For hypothesis one, three, four, five, seven in this study, factors which are change agents' promotion efforts, perceived attributes of VoLTE, communication channel, nature of social systems were found to have positive affect towards VoLTE adoption which was represent by adjusted R square 0.203 and 0.05 significant level, except substitution technology which was not affect.

REFERENCES

[1] Settapong Malisuwan, "LTE Transform-ation", Telecom & Innovation Journal, Vol. 23, No. 1008, pp. 3, 2015.

[2] Settapong Malisuwan, "From that day until today to 4G era", Telecom & Innovation Journal, Vol. 23, No. 1001, pp. 3, 2015.

[3] Ericsson Mobility Report, Traffic Exploration [Online], Available: http://www.ericsson.com/TET [2015, November 30].

[4] Global Mobile Suppliers Association (GSA), "4G Market & Technology Update", Evolution to LTE report, pp. 1, 2015.

[5] GSMA, IP Communication Statistics [Online]. Available: http://www.gsma.com/network2020/all-ip-statistics [2015, November 30].

[6] Sutisak Tantayotin, The Thailand Telecom-munications Indicators Year 2014-2015, Office of The National Broadcasting and Telecommunica-tions Commission, Thailand, 2015.

[7] Christopher Cox, "VoLTE and the IP Multimedia Subsystem", An Introduction to LTE: LTE, LTE-Advanced, SAE, VoLTE and 4G Mobile Communications, 2nd Edition, John Wiley & Sons, pp. 371-380, 2014.

[8] Ericsson, Voice and video calling over LTE [Online], Available: http://www.ericsson.com/res/ docs/whitepapers/wp-voice-and-video-calling-over-lte.pdf [2014, November 30].

[9] Everett M. Rogers, Diffusion of Innovation, 5th Edition, New York: Free Press, 2003.

[10] Everett M. Rogers & Floyd F. Shoemaker, Communication of Innovation; A Cross-Cultural Approach, New York: The Free Press, 1971.

IEET Editorial Office

EEAAT - Electrical Engineering Academic Association (Thailand)
Room 409, F-Building
140 Cheum-Sampan Rd.
Nong Chok, Bangkok, Thailand 10530
Tel: +662-988-3655 ext 2216 Fax: +662-988-4026

www.journal.eeaat.or.th